

# 4. Functional Imaging with Light-Sheet Microscopy

Raghav K. Chhetri

HHMI Janelia Research Campus

Philipp J. Keller

HHMI Janelia Research Campus

## 4.1 Introduction

Brain imaging techniques are essential for advancing our understanding of the basic principles underlying neural circuit function, connectivity across neuronal populations and entire brain regions, the functional development of the early nervous system and the mechanisms of neural circuits underlying behavior. The central tenet of imaging a nervous system in action is the spatiotemporal scale at which neuronal activity occurs, thereby setting it apart as a unique challenge rarely encountered in other bio-imaging scenarios. Additionally, imaging the activity from a population of neurons in the intact brain of a behaving animal makes this task even more challenging, which has motivated researchers to engage a variety of advanced techniques to push through this boundary. Among optical methods, light-sheet microscopy is well-positioned to tackle the numerous challenges encountered in functional imaging of the nervous system, as it provides a unique combination of strengths: light-sheet microscopy offers high spatial resolution, high imaging speed, good physical coverage of partially opaque specimens, and low energy load on the specimen for long-term imaging under physiological conditions. In this chapter, we discuss recent

efforts in recording neuronal activity using light-sheet microscopy and the opportunities it has carved in deepening our understanding of the inner workings of the brain.

## 4.2 Principles of Light-Sheet Microscopy

The conceptual foundation of light-sheet microscopy dates back to 1902 when Siedentopf and Zsigmondy developed a microscope, which they termed the “ultramicroscope”, to study scattering of visible light from sub-wavelength colloidal particles (Siedentopf and Zsigmondy, 1902). Unlike a traditional light microscope, the design of the ultramicroscope utilized an illumination beam orthogonal to the detection lens. This simple technical concept is the foundation of all modern light-sheet microscopy techniques, which rely on illuminating a thin section of a fluorescently labeled sample and collecting the emitted photons from the entire illuminated section along a detection axis positioned orthogonally to the illumination axis. This concept of separate illumination and detection, in combination with recent technical advancements in light sources, opto-mechanical components, fluorescent labels, detectors and computing frameworks, has positioned light-sheet microscopy as a powerful technique for fluorescence imaging in the life sciences.

Various high resolution optical techniques exist that can recapitulate the 3D extent of a physically sectioned sample (Osten and Margrie, 2013). However, methods that rely on physical sectioning obviously are not suitable for *in vivo* imaging. Thus, optical sectioning methods that leave the live specimen intact become necessary. Optical sectioning can be performed on images acquired from a standard epi-fluorescent microscope using post-processing algorithms to separate in-focus regions from out-of-focus regions. Confocal microscopes also perform optical sectioning by rejecting out-of-focus light using a confocal pinhole in the detection path. However, these methods always expose the entire depth of the sample to fluorescence excitation light which leads to

photobleaching and phototoxicity and can irreversibly damage the specimen when imaged over an extended period of time. Additionally, the rejection of out-of-focus light is not reliably achieved in highly scattering samples and is evident as a drop off in image contrast at larger depths. Light-sheet microscopy tackles these shortcomings of conventional techniques by implementing an efficient optical sectioning strategy that only illuminates a thin section of the specimen. The entire illuminated section is then rapidly imaged with a camera, which offers data acquisition rates that are several orders of magnitude higher than those achievable with point-scanning techniques. Volumetric imaging is achieved by sequentially illuminating different depth sections, and since signal photons are only emitted from a thin section of the sample at any time during this process, light-sheet microscopy also does not suffer as severely from background in highly scattering samples. Light-sheet microscopy thus outperforms conventional fluorescence microscopy techniques in its ability to rapidly image live specimens over an extended period of time with minimal photobleaching and phototoxicity while achieving excellent resolution and larger penetration depths.

There are many variations of light-sheet microscopy methods, and yet the general principle remains the same, as illustrated in **Figure 1**. The key approach in all light-sheet microscopes is the orthogonal illumination of a thin volume section with a “sheet” of light (Voie et al., 1993; Fuchs et al., 2002; Huisken et al., 2004) or with a rapidly scanning “pencil-beam” (Keller et al., 2008). Fluorescence light emitted by this thin section is then captured by a wide-field detection system to form an image. To acquire a 3D volumetric data set, either the sample is translated stepwise across a stationary light sheet or the light sheet is scanned step-by-step across a stationary sample to illuminate different volume sections (Ahrens et al., 2013). Iterating this 3D acquisition procedure then results in a temporal recording of the imaged volume.

#### 4.2.1 Live-Imaging of Multi-Cellular Organisms

Recent advances in light-sheet microscopy have made it possible to image complex multi-cellular organisms in their entirety while they undergo rapid morphological changes during their development (Keller et al., 2008; Tomer et al., 2012). The key in capturing such dynamics at the sub-cellular level across the entire biological system is achieving a favorable combination of the following factors: (1) high spatial resolution, (2) high temporal resolution, (3) good physical coverage of the specimen, (4) long-term imaging capability, and (5) low phototoxicity and photodamage. High spatial resolution ensures that neighboring cells and sub-cellular features are distinctly resolved in a multi-cellular organism. High temporal resolution is crucial for capturing fast dynamic processes such as cell shape changes and cell migration. Good physical coverage of the specimen is needed for a system-level analysis of whole-tissue morphogenesis and development of entire embryos. Long-term imaging capability is crucial to attain an uninterrupted track of the dynamic processes across the entire developmental timescale. Lastly, the interrogation of the biological specimen needs to be minimally invasive and should not disrupt the system under study, and as such, photobleaching and phototoxicity need to be kept at a minimum to avoid perturbing normal growth and development of the specimen. The number of photons emitted from the illuminated section of the specimen is the common resource all five of these parameters are competing for.

The low energy load in light-sheet microscopy experiments enables optimal utilization of the photon budget and affords whole-animal imaging with high spatial resolution and high temporal resolution at the same time. Experimental demonstrations to this end include high-resolution imaging of small multi-cellular organisms such as *Caenorhabditis elegans* (roundworm) embryos (Wu et al., 2013; Chen et al., 2014), invertebrates such as *Drosophila melanogaster* (fruit fly)

embryos/larvae (Tomer et al., 2012; Chhetri et al., 2015), and vertebrates such as *Danio rerio* (zebrafish) embryos/larvae (Keller et al., 2008; Chhetri et al., 2015). These samples encompass a wide range of physical sizes; the dimensions of *Caenorhabditis elegans* embryos are 50 x 30 x 30  $\mu\text{m}^3$ , *Drosophila melanogaster* embryonic dimensions are 500 x 200 x 200  $\mu\text{m}^3$ , and *Danio rerio* embryonic dimensions are 700 x 700 x 700  $\mu\text{m}^3$ . Owing to their different sizes, shapes, and levels of transparency, each of these animal models presents a unique imaging challenge and can be optimally tackled with a unique imaging solution. For instance, *C. elegans* embryos are small and transparent, and thus are ideal for imaging with short, thin light sheets (a few  $\mu\text{m}$ ) from one or at maximum two (orthogonal) views, as has been demonstrated using lattice light-sheet microscopy (Chen et al., 2014) and dual-view inverted selective plane illumination microscopy (diSPIM) (Wu et al., 2013).

Imaging large specimens such as zebrafish embryos that comprise a large, light-scattering central yolk cell and partially opaque specimens such as *Drosophila* embryos presents additional challenges with limited depth penetration that cannot be resolved using lattice light-sheet microscopy and diSPIM. Additionally, the use of short, thin light sheets may not be ideal in these large specimens since temporal resolution must be sacrificed to acquire the large number of images that are needed to cover the entire specimen volume. Thus, imaging these large vertebrate and higher invertebrate embryos at high temporal resolution necessitates using longer, slightly thicker light sheets which consequently reduces axial resolution across the imaging volume. However, this reduction in axial resolution can be recovered by combining the usage of thicker light sheets with orthogonal multi-view imaging (Swoger et al., 2007), which facilitates the reconstruction of a 3D image of the specimen with near-isotropic resolution. The acquisition of at least four

orthogonal views (comprising two sets of pairwise opposing views of the sample) additionally improves physical coverage of large, non-transparent specimens.

#### 4.2.2 Imaging at High Spatiotemporal Resolution

First-generation laser light-sheet fluorescence microscopes acquired volumetric data by translating the sample sequentially across the stationary light-sheet and detection focal plane. These setups utilized motorized stages that can translate as well as rotate the mounted specimen, and were used quite successfully for long-term developmental imaging with relaxed temporal sampling requirements. To image processes that demand higher spatiotemporal resolution, the physical scanning of the specimen is often slow and thus inadequate. Increasing the scanning speed of the (typically rather soft) specimen introduces motion artifacts in the acquired images, but more importantly, also has the potential to perturb the physical state of the specimen, particularly in long-term imaging applications. In order to achieve a higher temporal resolution, instead of translating the specimen for depth-sectioning, both the detection focus and the light sheet can be synchronously translated across a stationary specimen. This scheme typically utilizes a combination of high-speed piezoelectric scanners to translate the detection objectives and galvanometric mirrors to synchronously position the light sheet coplanar with the detection focal plane (Ahrens et al., 2013). A physical rotation of the specimen can then facilitate the acquisition of multi-view image data and subsequent reconstruction of images with isotropic resolution, as was demonstrated by imaging *Drosophila* and zebrafish embryos (Swoger et al., 2007). However, due to the inherent delay in rotating the specimen in multiple orientations, some of the faster cellular dynamics can potentially still be missed or temporally under-sampled, thereby making it difficult to accurately register information from multiple views during post-processing. The limitation of inadequate temporal resolution in multi-view imaging of large specimens at a high

spatial resolution was recently addressed using isotropic multi-view light-sheet microscopy (IsoView) (Chhetri et al., 2015). IsoView addresses the issue of attaining sub-cellular, isotropic resolution while retaining high temporal resolution in light-sheet imaging of large, non-transparent specimens (up to  $800 \times 800 \times 800 \mu\text{m}^3$  in size). IsoView utilizes an orthogonal arrangement of four shared illumination and detection objectives (**Figure 1**). As such, the lateral and axial dimensions, along which resolution are high and low, respectively, are permuted for orthogonal imaging arms. Thus, the registration of the image content from the four views and subsequent multi-view deconvolution results in near-isotropic volumetric data, with a system resolution of 400-450 nm in all spatial dimensions. IsoView enables fast-volumetric imaging via three unique modes of imaging – (1) sequential imaging of orthogonal views, (2) simultaneous imaging of orthogonal views using non-overlapping emission spectra, and (3) simultaneous four-view imaging by spatially offsetting the orthogonal light-sheet scans in the vertical direction and matching the active row of pixels in the respective sCMOS detectors operated in confocal line-scanning mode. To demonstrate the utility of IsoView for fast developmental imaging, simultaneous two-color imaging was performed in a gastrulating *Drosophila* embryo at a volumetric rate of 0.25 Hz (75 planes/volume for each view, acquiring 8 views in total), which offered not only high enough temporal resolution to capture key events during gastrulation but also isotropic,  $\mu\text{m}$ -level resolution for reliably distinguishing neighboring cells and morphological features across the entire embryo.

### **4.3 Functional Imaging of the Nervous System using Light-Sheet Microscopy**

Recently engineered genetically encoded calcium indicators (GECIs), such as GCaMPs, RCaMPs etc., that change fluorescence levels depending on calcium concentration allow neuronal activity to be measured optically (Looger and Griesbeck, 2012). Unlike whole-cell patch clamp

electrophysiology, which constitutes a direct measurement of neuronal activity, calcium imaging is an indirect measure from which neuronal spiking activity can be extracted. The basic working principle in calcium imaging is the influx of calcium during an action potential of a neuron followed by a quick restoration of the resting potential as calcium is returned to the extracellular space and the compartments in the endoplasmic reticulum. This brief surge of calcium, which is reported by GECIs, thus represents an indirect activity measure for a firing neuron. Although whole-cell patch clamping is still considered the gold standard in measuring neuronal activity, it is often not ideally suited to recapitulate how different parts of a neuron interact or how assemblies of neurons communicate. Recording neuronal activity using optical methods overcomes these shortcomings and offers several advantages. First, imaging neuronal activity is less invasive than inserting electrodes directly onto a cell, which can irreversibly damage the cell. Second, optical imaging facilitates gathering data from a much larger population of neurons, thereby enabling correlative analysis of activities across different neuronal sub-populations and brain regions. Lastly, optical methods also provide anatomical information and enable pairing of neuronal activity with cell identity when neurons expressing calcium sensors are co-labeled for cell types. Although various optical techniques (Wilt et al., 2009) exist for recording from multiple neurons, the number of simultaneously recorded neurons in the brain of the animal is typically small. This constraint primarily arises from limitations in the speed at which volumetric data can be collected across the brain of an animal.

Recording the activity from a population of neurons demands much higher acquisition speeds than a majority of dynamical processes encountered in developmental imaging. Various high-speed optical imaging modalities, such as two-photon point-scanning microscopy, two-photon random access microscopy and light-field microscopy among others, aim to meet the demands of high

spatiotemporal resolution in neuronal imaging, and each offer distinct advantages and utility. Two-photon microscopy, which confines fluorescence excitation to the illumination focus, excels at imaging inside scattering tissues and captures images with high spatial resolution at depths inaccessible to conventional single-photon techniques. However, two-photon point scanning microscopy requires the excitation spot to be sampled sequentially across the entire imaging volume, which limits the overall volumetric acquisition speed. In sparsely labeled samples, the speed bottleneck of two-photon imaging is overcome by two-photon random access microscopy, which samples a limited number of spots distributed across a large sample volume, thereby increasing the temporal rate at which the regions of interest are sampled (Grewe et al., 2010; Sofroniew et al., 2016). Light field microscopy, in which the spatial and angular distributions of the emitted fluorescent light are captured simultaneously using a microlens array positioned conjugate to the image plane, acquires volumetric information from the entire sample volume onto a single camera chip and thus offers exceptionally high volumetric acquisition speed (Levoy et al., 2006; Prevedel et al., 2014). However, the compression of the entire light-field onto a single two-dimensional sensor reduces the spatial resolution across the acquired volume, which often constrains the interrogation of neuronal activities to a local group of neurons instead of single neurons. Compared to these complementary high-speed neuroimaging techniques, light-sheet microscopy offers a unique approach for large-scale *in vivo* recording of neural activity in transparent and small non-transparent samples at high spatiotemporal resolution and over an extended period of time.

Below we discuss various recent implementations of light-sheet methods in imaging neuronal activity in zebrafish, *Drosophila*, and mammalian brains.

### 4.3.1 Light-Sheet Functional Imaging in Zebrafish

The larval zebrafish is an excellent model organism for studies in developmental biology and neuroscience. Owing to its compact size and transparency, zebrafish naturally lend themselves to optical imaging and have thus been used for numerous imaging-based studies in developmental biology and neuroscience. The suitability of zebrafish for light-sheet imaging combined with the availability of GECIs in larval zebrafish has made it possible to image activity in large population of neurons across the zebrafish brain. Panier et al. and Ahrens et al. first demonstrated the utility of light-sheet microscopy for functional imaging in larval zebrafish, and captured single-neuron level functional activity from thousands of neurons in the zebrafish brain (Ahrens et al., 2013; Panier et al., 2013) (**Figure 2a-f**). Panier et al. used GCaMP3 to label the neurons in the brain of 5-9 dpf larval zebrafish, and performed light-sheet imaging by paralyzing the zebrafish and embedding them in 1.8% agarose. In this study, the authors demonstrated functional recording from about 30% of the neurons across the brain by sequentially sampling 5 image planes (with a separation of 8  $\mu\text{m}$  between planes) at a volumetric rate of 4 Hz. A functional recording from a single z-plane at a repetition rate of 10-20 Hz was also demonstrated for a duration of 30-60 minutes. Although one third of the entire brain was imaged in this study, volumetric imaging was performed by rapidly moving the sample (followed by a short pause after each movement to allow the specimen to come to rest) and thus constituted a limiting factor in attaining a finer depth sectioning across the entire brain while maintaining the same high volumetric imaging rate. Ahrens et al. instead employed piezo-based volumetric imaging, which allows keeping the specimen stationary and moving the light sheet and detection objective in synchrony. In this latter study, the authors recorded activity from the entire volume of the brain of a GCaMP5G labeled larval zebrafish at 0.8 Hz (41 z-planes/volume with the planes 5  $\mu\text{m}$  apart), covering more than 80% of

all neurons at single-cell resolution. These imaging experiments captured for the first time single-neuron level functional activity across almost the entire brain volume of  $800 \times 600 \times 200 \mu\text{m}^3$  in an intact, live vertebrate. Thereby, this study demonstrated a key advantage of light-sheet microscopy in interrogating neuronal activity patterns in disparate brain regions and subsequently allowing characterization of correlations across the entire brain. These computational analyses revealed two functionally defined neuronal circuits, termed the hindbrain oscillator and the hindbrain spinal circuit.

For studies relying on visual stimulus to generate behavior, the experimental setups in Panier et al. and Ahrens et al. leave the retinas of the zebrafish exposed to the excitation light, which can disrupt behavior and neural processing. To circumvent this problem, Vladimirov et al. presented a scheme that avoids scanning the laser beam across the eyes of the zebrafish and thus prevents direct stimulation of the photoreceptors by the imaging laser (Vladimirov et al., 2014) (**Figure 2g-i**). The authors were then able to present a visual stimulus via a projection screen in the larval zebrafish's field of view and simultaneously monitor the cellular-level neural activity during visual-motor behavior using the expression of cytoplasmic GCaMP6s. Near-complete coverage of the entire brain in the fictively behaving larval zebrafish was obtained at a high volumetric rate of 3 Hz (40 z-planes/volume with the planes separated by  $5 \mu\text{m}$ ) in this study. The authors successfully captured forward optomotor responses initiated by the movement of the grating pattern projected onto the screen, and also tested the adaptation of the zebrafish's motor output in response to the strength of the visual signal. An alternative light-sheet imaging approach for avoiding the activation of the retinas and other photosensitive cells was presented by Wolf et al. (Wolf et al., 2015) (**Figure 2j,k**). This approach relies on two-photon excitation, using a light sheet at a wavelength of 930 nm in order to significantly reduce the response of the fish's visual system to

light-sheet illumination. Visual stimulation was presented in the form of a series of blue flashes of increasing intensity, and the flash-evoked neuronal activity in the brain of a zebrafish larva expressing GCaMP5G was recorded at a volumetric rate of 1 Hz (9 z-planes/volume with the planes 8  $\mu$ m apart). Additionally, the authors presented a direct comparison of flash-evoked response when imaging is carried out using single-photon versus two-photon excitation. In order to obtain similar contrast and signal-to-noise ratios, average laser powers on the order of several 100 mW and several 100  $\mu$ W were needed for two-photon excitation and one-photon excitation, respectively. A 4 Hz single-plane recording showed that the flashes evoked stronger responses in various regions of the brain during two-photon imaging compared to single-photon imaging, which establishes two-photon light-sheet microscopy as a useful alternative for functional imaging assays that require minimizing the possible impact of the laser illumination beam on neural processing.

Alternatives to high-speed piezo scanning for volumetric imaging have also been explored for light-sheet microscopy (Tomer et al., 2015; Quirin et al., 2016) (**Figure 3**). These approaches involve extending the depth of field of the detection optics (Zalevsky and Ben-Yaish, 2007; Mouroulis, 2008) and attaining depth-sectioning by simply scanning the light sheet across the sample. These approaches thus leave the local vicinity of the specimen motion-free as the detection objective remains stationary and also offer a way to image from a select few arbitrary regions within the imaging volume at a high repetition rate (Quirin et al., 2016). Similar to piezo-based high-speed light-sheet microscopes, the speed in these approaches are also currently limited by the frame rate of the detector, the pixel dwell time required to collect images at a reasonable SNR, and most importantly, the photon budget and light tolerance of the specimen. One such approach applied to neuronal imaging in larval zebrafish is SPED (Spherical-aberration-assisted Extended Depth-of-field light-sheet microscopy) (Tomer et al., 2015). In this method, the depth of field is

extended by inserting a thick block of optical material with an altered refractive index ( $n = 1.454$ ) in between the detection objective and the sample, which in effect introduces a large spherical aberration and elongates the detection point-spread-function (PSF) (**Figure 3c,d**). In this manner, as the light sheet is scanned across the sample, an image volume is captured with the stationary detection objective. At 4x magnification, the authors demonstrated 12 Hz imaging (40 z-planes/volume with 5  $\mu\text{m}$  separation between adjacent planes) of the brain and 6.23 Hz imaging (39 z-planes/volume with 5  $\mu\text{m}$  separation between adjacent planes) of the central nervous system (CNS) including the spinal cord in GCaMP6s-expressing zebrafish larva. The authors also demonstrated 4.14 Hz imaging (39 z-planes/volume with 5  $\mu\text{m}$  separation between adjacent planes) of the brain and spinal cord at a slightly higher magnification of 10x. It should be noted that, unlike other light-sheet microscopy techniques, SPED critically relies on detection objectives with low numerical apertures (NA of 0.25-0.28), since the z-range of the SPED imaging volume depends fundamentally on the numerical aperture of the objective. Since the photon efficiency of the imaging system is proportional to the square of the numerical aperture, SPED imaging thus taxes the photon budget, which in turn limits spatiotemporal resolution and increases photo-toxicity and photo-damage. The microscope's lateral resolution, which is proportional to the numerical aperture of the detection objective, is degraded for the same reason. Extended depth-of-field imaging furthermore reduces axial resolution (from around 2  $\mu\text{m}$  in conventional functional imaging experiments to around 5  $\mu\text{m}$  in SPED), since axial resolution is only determined by the illumination PSF in SPED. Another extended depth-of-field approach applied to neuronal imaging in larval zebrafish involves the use of a cubic phase mask (Dowski and Cathey, 1995) in the detection path of a light-sheet microscope (Quirin et al., 2016) (**Figure 3a,b**). In this method, the wavefront is encoded with a spatially dependent phase retardation, and a high-resolution

volumetric data set is recovered via deconvolution using the PSFs that result from system modulation with the cubic phase mask. Unlike SPED, in which the induced spherical aberrations become non-linear for high-NA objectives, the extension of the depth-of-field using a phase mask does not pose any limitation on the NA of the detection objective. As such, high-NA objectives (e.g. NA of 0.8 used in Quirin et al.) can be utilized, offering a higher photon efficiency and also collecting higher spatial frequencies from the sample that are otherwise missed in SPED (NA of 0.25- 0.28 used in Tomer et al.). Using the cubic-phase-mask aided light-sheet microscope, Quirin et al. imaged the brains of zebrafish larvae expressing GCaMP6s or GCaMP6f at a volumetric rate of 1.5 Hz (40 z-planes/volume with the planes 5  $\mu$ m apart) in the presence of periodic visual stimuli. Owing to the ability to access arbitrary planes quickly, the authors were also able to image from three axial planes across an axial range of 160  $\mu$ m at a repetition rate of 33 Hz.

Although the transparency of zebrafish is a great match for light-sheet microscopy, the relatively large size of these specimens often makes it challenging to maintain high resolution and high contrast particularly at larger imaging depths. Maintaining these factors at a high volumetric imaging rate further complicates this task. Recently, we presented an effective strategy for high-speed, isotropic multi-view imaging with the development of IsoView microscopy (**Figure 4a**). Using IsoView, four-view image data of the whole brain of a larval zebrafish expressing GCaMP6s was acquired at a volumetric rate of 1 Hz (67 planes/volume for each view, with 6  $\mu$ m separation between adjacent planes), which captured large-scale brain activity and reliably resolved neighboring cells even in the deep regions of the brain. **Figure 4b** shows high-resolution images acquired using IsoView, contrasted against images acquired using conventional light-sheet methods. A closer look at the deep regions outlined in **Figure 4b** shows that IsoView microscopy reliably distinguishes neighboring cells even in such deep regions (**Figure 4c**) and thus faithfully

captures the activity traces of single neurons that frequently suffer from signal cross-talk between neighbors in conventional light-sheet imaging.

To obtain high-resolution images of living specimens at all spatial locations and over long periods of time (hours to days) adds another layer of difficulty, since the optical properties of complex multi-cellular organisms are not only heterogeneous across the specimen volume but also change significantly over time. Consequently, the spatial overlap of light sheets and detection focal planes, which is crucial for recording high-resolution images in light-sheet microscopy, suffers and thus spatial resolution and contrast in the images are degraded. Recovering and maintaining perfect co-planarity of light sheets and the detection focal planes requires an imaging framework that automatically adapts to these changing imaging conditions. Such a framework for spatiotemporally adaptive imaging has recently been developed and released as the open-source *AutoPilot* project (Royer et al., 2016). This framework consists of (1) a multi-view light-sheet microscope capable of digitally adjusting the positions of detection planes as well as the positions and angles of light sheets in three dimensions, and (2) a software control layer that monitors and continuously optimizes image quality across the specimen volume in real-time (**Figure 4e**). Using this spatiotemporally adaptive light-sheet microscope, whole-brain functional imaging in zebrafish larva expressing nuclear-localized GCaMP6f across the nervous system has been demonstrated at a volumetric rate of 3 Hz (41 planes/volume with 5  $\mu\text{m}$  separation between adjacent planes) over a period of 24 hours. Spatial resolution and contrast in the adaptively corrected images are substantially improved compared to the uncorrected image data (**Figure 4f**): the *AutoPilot* framework maintains high image quality even across a sample volume as large as the zebrafish larval brain and recovers cellular and sub-cellular structures in many anatomical regions that are not resolved by conventional, non-adaptively light-sheet microscopy.

### 4.3.2 Light-Sheet Functional Imaging in *Drosophila*

The fruit fly *Drosophila melanogaster* is a popular model organism in neuroscience due to its small size, genetic tractability, the availability of a powerful arsenal of genetic tools, its remarkable repertoire of complex behaviors, and its importance as a model system for many neurodegenerative diseases. Light-sheet microscopy has recently expanded the utility of fluorescence imaging in *Drosophila* embryos by parallelizing the acquisition of multi-view image data in long-term live imaging experiments of *Drosophila* developmental dynamics. Unlike zebrafish, *Drosophila* embryos and larvae are partially opaque and exhibit higher cell densities in many parts of their central nervous system, which presents a challenge for volumetric imaging at high resolution despite their relatively smaller size. Building upon SiMView light-sheet microscopy (Tomer et al., 2012), Lemon et al. designed a high-speed microscopy framework for multi-view functional imaging (hs-SiMView) with one-photon and two-photon excitation, and successfully demonstrated functional imaging of neural activity across entire nervous system explants of third-instar *Drosophila* larvae (approximately 500 x 200 x 200  $\mu\text{m}^3$  in size), utilizing two opposing sCMOS cameras for streaming multi-view volumetric image data at a sustained data rate of 1 GB/s (Lemon et al., 2015). This method involved simultaneously imaging from two opposing views to overcome the limited physical coverage achieved with single-view imaging in a highly light-scattering sample such as the CNS of *Drosophila* (**Figure 5a**). To attain rapid optical sectioning, the light sheets were swept using galvanometer scanners and the detection focal planes were synchronously moved across a stationary specimen using high-speed piezo positioners. Using one-photon excitation, the authors demonstrated 5 Hz (37 z-planes/camera with 4-6  $\mu\text{m}$  separation between adjacent planes) volumetric imaging for a 1-hour period in *Drosophila* third instar larval CNS explants expressing GCaMP6s. Using two-photon excitation (940 nm) volumetric imaging

was demonstrated at a volume rate of 2 Hz for a 1-hour period. The two-photon assay thus complements the faster 5 Hz single-photon recording capabilities (488 nm) with an imaging mode that sacrifices temporal resolution but improves depth penetration and signal-to-background ratio. This work constitutes a first demonstration of functional imaging of neuronal activity at near cellular resolution throughout the entire CNS of a higher invertebrate (**Figure 5c,d**). A further improvement in resolution and isotropy was achieved with the development of IsoView microscopy (Chhetri et al., 2015). Using IsoView, we recently performed whole-animal functional imaging of late-stage *Drosophila* embryos expressing GCaMP6s throughout the nervous system at a volumetric rate of 2 Hz (40 planes/volume with 5.2  $\mu\text{m}$  separation between planes; 4 views/volume). In these experiments, we recorded whole-nervous-system activity patterns associated with various motor behaviors such as forward crawling, backward crawling, and turning. The high, isotropic resolution afforded by IsoView was evident throughout the nervous system, as axon bundles, neighboring cell somas and in some instances even individual axons were distinctly resolved, even during fast specimen movements. **Figure 5e** shows dorsal- and lateral-view projections of an embryo imaged with IsoView. A closer look at a deep region in the ventral nerve cord (**Figure 5f**) demonstrates the high-resolution of IsoView image data in all three dimensions and shows that neighboring soma with a diameter of 2-3  $\mu\text{m}$  are resolved as separate structures. IsoView also affords long-term functional imaging capability, which was demonstrated by performing functional imaging of an entire *Drosophila* embryo over developmental time scales: development and functional maturation of the nervous system were captured from the onset of neuronal cell differentiation up to the first-instar larval stage at a volumetric rate of 2 Hz (35 planes/volume with 6.8  $\mu\text{m}$  separation between planes; 4 views/volume) over a 9-hour period, at the end of which the fully formed larva crawled out of the imaging volume.

Functional *in vivo* imaging in adult *Drosophila* was also recently demonstrated using objective-coupled planar illumination (OCPI) microscopy (Liang et al., 2016) (**Figure 5g**). OCPI is a light-sheet microscopy method in which a miniaturized illumination arm is coupled directly to the detection objective, and the light sheet is generated using a beam passing through a single-mode optical fiber, a light collimator, and a cylindrical lens (Holekamp et al., 2008). In this method, as the piezo-positioner moves the detection objective for depth-sectioning, the illumination sheet moves along with it as a result of the physical coupling, and thus offers a geometrically compact alternative to three-dimensional imaging without physically moving the sample or scanning the light sheet. Additionally, to minimize optical path lengths in the sample, both the illumination and detection axes are tilted approximately by 45° with respect to a horizontally mounted sample. To perform OCPI imaging of the brains of living adult flies, the authors made cranial holes and monitored GCaMP6s fluorescence in five of the eight major pacemaker neurons over a duration of 24 hours. Using volumetric stacks obtained in 10-minute intervals for 24 hours, the authors were able to identify a systematic change in calcium dynamics in pacemaker neurons as a function of the time of day (**Figure 5h**).

#### 4.3.3 Light-Sheet Functional Imaging in Mammalian Brains

A majority of functional imaging with light-sheet microscopy in the mammalian brain has thus far been performed on *ex vivo* tissues. Using OCPI (**Figure 6a**), Holekamp et al. demonstrated the utility of light-sheet microscopy in imaging regions of mammalian brains by capturing fast calcium dynamics from a population of neurons up to a depth of 150 µm from the surface of an excised tissue (Holekamp et al., 2008). This work not only represents the first application of light-sheet microscopy to live imaging of mammalian neural tissues but it also marks the first use of light-sheet microscopy for functional imaging in general. In this study, intact vomeronasal epithelium

from male mice, labeled with the calcium-sensitive fluorescent dye Oregon green BAPTA-1, was excised and imaged using OCPI microscopy to study the pheromone-sensing neurons of the mouse vomeronasal organ (VNO) in response to chemical stimulation (**Figure 6b**). By scanning the plane of illumination in tandem with the detection focal plane at a volumetric rate of 0.167 Hz (40-50 z-planes/stack with 5  $\mu\text{m}$  separation between the planes; each stack acquired in 2 seconds), the authors were able to simultaneously record the response of hundreds of VNO neurons to chemical stimulation for up to a few hours. Holekamp et al. furthermore monitored calcium dynamics in 88 cells within a single field of  $700 \times 100 \mu\text{m}^2$  at a repetition rate of 200 Hz, capturing small changes (~0.2%) in fluorescence due to spontaneous activity of the neurons. Building upon this original demonstration, the investigators further visualized neuronal activity via the expression of GCaMP2 across the entire depth of the vomeronasal epithelium at a volumetric rate of 0.2 Hz (40 z-planes/stack with 5  $\mu\text{m}$  separation between the planes; each stack acquired in 2 seconds), typically over a duration of ~1 hour (Turaga and Holy, 2012). In this case, the time-lapse image data of the  $700 \times 175 \times 200 \mu\text{m}^3$  tissue volume captured spontaneous and chemical-stimulus-driven activities from thousands of sensory neurons. In a recent study, even larger image volumes ( $713 \times 712 \times 400 \mu\text{m}^3$ ) of the mouse accessory olfactory bulb (AOB) were acquired using OCPI at a volumetric rate of 0.2 Hz (50 z-planes/stack with 8  $\mu\text{m}$  separation between the planes) (Hammen et al., 2014). These image stacks covered the entire anterior AOB and a third of the posterior AOB. To probe the connectivity of the VNO to the AOB, the authors delivered chemical stimuli to the VNO and recorded the subsequent response in the densely packed glomerular layer of the AOB using GCaMP2 for a duration of up to 1 hour and 40 minutes. To analyze the roles of neuronal cell types present in mice in relation to gender, hormones, and sensory experience, a large-scale recording from approximately 10,000 neurons expressing GCaMP2 or GCaMP3 in the VNO was recently

demonstrated using OCPI (Xu et al., 2016). In this study, the authors imaged two intact VNO regions ( $710 \times 125 \times 282 \mu\text{m}^3$ ), constituting about one-seventh of the entire VNO tissue volume, for a total of 26 VNO preparations, and identified 17 physiological types of vomeronasal neurons. These studies constitute an illustration of fast, comprehensive, *ex vivo* neuronal recordings of anatomically inaccessible regions of a mammalian brain, such as the VNO and the AOS, over an extended duration using light-sheet microscopy.

Light-sheet microscopy has the potential to be a mainstay for high-speed imaging in laboratories studying organotypic slices of mammalian brains, especially considering the extensive resources to build low-cost systems afforded by the openSPIM project (Pitrone et al., 2013). Recently, a compact inverted light-sheet microscope, based on the openSPIM design, was presented and successfully applied to the imaging of calcium dynamics in brain slices of rat pups (Yang et al., 2016). In this study, glutamate-uncaging-evoked calcium transients were captured in two-dimensional time-lapse images acquired at a frame rate of 200 Hz. Additionally, action-potential-evoked calcium influx along an axon in an organotypic rat hippocampal slice virally infected by GCaMP6s was also recorded as a two-dimensional time-lapse at a frame rate of 30 Hz. Contrasted with conventional methods for recording calcium transients in which a line-scan is performed over a predefined region, this method enabled calcium transients to be recorded across the entire two-dimensional area, thereby capturing events that would have otherwise been missed.

Unlike in zebrafish and *Drosophila*, the geometry of light-sheet microscopes with orthogonal illumination and detection objectives limits access to an intact mammalian brain for *in vivo* imaging. Thus, methods that can generate a tilted light-sheet and image fluorescence with a single objective are required to probe the neurons in a live mammalian brain. One such solution was recently introduced as a light-sheet design termed SCAPE (Swept, Confocally-Aligned Planar

Excitation) microscopy (Bouchard et al., 2015). Unlike most other light-sheet microscopes, SCAPE utilizes a single objective for oblique light-sheet illumination as well as detection from the light-sheet plane (**Figure 6c**). Thus, a single, stationary objective configuration of SCAPE makes sample positioning and alignment as simple as in conventional upright or inverted microscopes. SCAPE microscopy implements a unique scanning and de-scanning scheme, such that a scanning polygonal mirror located behind the objective sweeps the light sheet across the sample and an adjacent facet of the same polygonal mirror de-scans in the imaging path, thereby capturing images of the optically sectioned illumination planes without any physical translation of the objective or the sample. Using SCAPE, the authors imaged superficial cortical layers ( $350 \times 800 \times 105 \mu\text{m}^3$ ) in head-fixed, awake mice expressing GCaMP6f in layer 5 pyramidal neurons at a volumetric rate of 10 Hz (100 angular sampling steps in  $350 \mu\text{m}$ ), and demonstrated spontaneous calcium transients in superficial dendrites (**Figure 6d**). Additionally, a large volume ( $600 \times 650 \times 134 \mu\text{m}^3$ ) of the superficial cortex in a head-fixed, awake mouse expressing GCaMP5G in layer 5 pyramidal neurons was also imaged for a duration of 180 seconds at a volumetric rate of 10 Hz (240 angular sampling steps in  $600 \mu\text{m}$ ) using 2x2 camera binning. Upon subsequent analysis of the calcium onset and decay dynamics, the authors were able to reliably differentiate dendrites in the imaged volume based on their unique firing dynamics. These image data of the brain of awake mice illustrate the utility of SCAPE microscopy for rapid volumetric imaging in the superficial layers of the cortex. In the present implementation of SCAPE microscopy, the authors show that spatial resolution is worse than for two-photon microscopy, even in superficial regions of the mouse cortex, but they also demonstrate that SCAPE does offer sufficient spatial resolution for meaningful analyses of neuronal dynamics at substantially higher sampling rates.

#### 4.4 Performance and Design Choices

Whole-brain functional imaging experiments stand out among other types of light-sheet microscopy experiments in particular with respect to their unique performance requirements. Calcium imaging of entire zebrafish larval brains, *Drosophila* larvae or mammalian neural tissues requires scanning relatively large volumes (typically ranging from 500 x 200 x 200  $\mu\text{m}^3$  to 800 x 500 x 400  $\mu\text{m}^3$  or more) at high volumetric imaging rates of at least 1 Hz, ensuring proper temporal sampling of the calcium indicator. At the same time, it is desirable – if not crucial – to achieve high spatial resolution in order to ensure that the functional activity of individual neurons can be reliably distinguished from the activity of their respective neighbors. When executing complex experimental workflows involving e.g. behavior assays with multiple measurement conditions, long-term imaging capability may furthermore be essential for the successful acquisition of a meaningful data set. Achieving this combination of high temporal resolution and high spatial resolution across a large imaging volume over extended periods of time poses technical challenges and requires careful consideration of the most appropriate microscope design choice in each experiment. Further difficulties can arise when performing behavioral assays that require avoiding exposure of the specimen to excitation laser light at visible wavelengths or when working with specimens that do not offer optical access from two orthogonal directions. In this section we will discuss the main performance criteria outlined above, the capabilities and limitations of different approaches and the general performance implications of using certain types of light-sheet microscope designs. A performance comparison of various light-sheet microscopes discussed in this chapter is summarized in **Table 1**.

### *Temporal resolution*

The primary speed bottleneck in state-of-the-art light-sheet microscopes is camera performance. Irrespective of the volume imaging strategy used in a particular light-sheet microscope implementation, limitations in camera frame rate are the first obstacle that is encountered in the imaging workflow when striving to maximize data rates. Two-photon light-sheet microscopy currently represents the only exception to this rule; in this latter case, the primary limitation is the signal rate, as will be discussed further below.

For example, high-speed, high-resolution functional imaging of a zebrafish brain volume of 830 x 500 x 400  $\mu\text{m}^3$  with IsoView light-sheet microscopy is limited to a volume rate of 2 Hz, since the corresponding data rate (340 million voxels per second) marks the performance limit of the microscope's Orca Flash 4.0 sCMOS cameras: considering an overhead of at least 1 ms per frame to accommodate the finite exposure time, the camera operates at a duty cycle of >90% in this scenario (Chhetri et al., 2015). Of course, it is possible to increase this volume rate beyond 2 Hz by sacrificing spatial resolution. This decision in turn allows using a smaller image frame size and thus an accordingly higher frame rate. An example to this end is zebrafish whole-brain functional imaging with SPED microscopy, covering a 900 x 400 x 200  $\mu\text{m}^3$  volume at 12 Hz (Tomer et al., 2015). The 2.6-fold increase in volume rate in this example (note that the IsoView imaging volume is 2.3-fold larger) is not related to the different volume scanning approach used in SPED but rather the result of a reduction in spatial sampling and spatial resolution: the SPED experiment is performed at 4x magnification and acquires images of the brain with a frame size that is 18.5-fold smaller than the respective frame size in IsoView (which uses the same camera model but employs a higher, 16x magnification). If we also consider that raw axial resolution is 2-fold lower in SPED, it follows that the 3D size of voxels in the raw image data is 32-fold larger in SPED than in

IsoView. Despite the higher volume rate, the data throughput in the SPED experiment is in fact only 65 million voxels per second, i.e. this SPED experiment provides 5-fold lower data throughput than e.g. a single detection arm of the IsoView microscope.

It should be noted that there are several misconceptions regarding the sources of limitations in volumetric imaging rates in light-sheet microscopy. In particular, the notion that imaging rates are currently not only limited by camera performance but also by piezo performance when using piezo-based volume scanning is incorrect. Even for the heaviest, highest-performing detection objectives (such as custom objective designs that combine high numerical apertures with large working distances, weighing in typically at 300-500 g), volume rates of 20 Hz are in principle feasible for a 250  $\mu\text{m}$  travel range and 10 Hz for a 750  $\mu\text{m}$  travel range. As outlined above, when acquiring well-sampled, high-resolution volumetric image data piezo performance thus surpasses the data throughput capabilities of existing sCMOS camera technology approximately 10-fold. Moreover, when using low-weight, low-NA objectives (such as those used in SPED), existing piezo technology offers even higher volume rates, ranging up to several hundred Hz for 200-900  $\mu\text{m}$  travel ranges (e.g. Piezosystem Jena piezo models nanoX 200/400 and nanoSX 400/800).

Importantly, although alternative volume imaging approaches that avoid piezo scanning can be advantageous when it is necessary to minimize motion in the vicinity of the sample, these approaches inherently suffer from several critical disadvantages. Possible alternatives to piezo scanning include the use of electric tunable lenses for remote focusing (Fahrbach et al., 2013), swept oblique light sheet imaging (Bouchard et al., 2015) as well as extended depth of field imaging mediated by spherical aberrations (Tomer et al., 2015) or pupil encoding with cubic phase masks (Quirin et al., 2016). Microscope designs using electric tunable lenses suffer from the fact that optical quality of tunable lenses is lower than that of conventional lenses and image quality is

additionally reduced when deviating significantly from the design working distance of the detection objective. This latter issue is also encountered in microscope designs utilizing swept oblique light-sheet imaging and pupil encoding with cubic phase masks. Extended depth of field imaging mediated by spherical aberrations or pupil encoding with cubic phase masks also reduces axial resolution because it eliminates the contribution of the detection objective to the axial component of the microscope's PSF. Axial resolution is thus reduced 2-3 fold in SPED and in light-sheet imaging with cubic phase masks when compared to piezo-based volumetric imaging. SPED furthermore suffers from a reduction in lateral resolution and photon-efficiency as it is intrinsically limited to the use of low-magnification objectives with low numerical aperture. A typical SPED whole-brain functional imaging experiment with a 4x/0.28NA objective reduces sampling-limited lateral resolution 5-fold and photon-collection efficiency 13-fold compared to a conventional piezo-based whole-brain functional imaging experiment with a high-quality 20x/1.0NA objective (Ahrens et al., 2013). Finally, it should be noted that with the advent of more advanced camera technology the bottleneck in future generations of light-sheet microscopy will shift from maximum camera speed to the maximum achievable fluorescence signal rate under physiological conditions. As volumetric imaging rates increase, accordingly higher laser power densities are needed to maintain the same signal-to-noise ratio under otherwise identical imaging conditions (i.e. assuming that spatial resolution and spatial sampling are maintained as well). The speed of image acquisition will thus ultimately be limited by the saturation of fluorophores and the maximum light dose the biological specimen tolerates.

### *Spatial resolution*

Performance with respect to spatial resolution varies substantially over the current spectrum of light-sheet microscopy techniques for functional imaging. Of course, it is generally desirable to

achieve high resolution in any study that requires faithful measurement of neuronal activity at the single-cell level. Achieving this goal, however, is complicated by the need to image a relatively large field-of-view in typical whole-brain functional imaging studies. At the core of this issue is the fact that resolution is highly anisotropic in conventional light-sheet microscopy for large field-of-view imaging, i.e. axial resolution is often 5- to 10-fold worse than lateral resolution (Ahrens et al., 2013; Panier et al., 2013; Lemon et al., 2015; Tomer et al., 2015; Wolf et al., 2015; Quirin et al., 2016). There are currently only a handful of techniques that overcome this particular limitation and offer high lateral as well as high axial resolution. Unfortunately, most of these techniques rely on principles that increase spatial resolution at the expense of temporal resolution, which makes them intrinsically unsuited to large-volume functional imaging. For example, Bessel beam and lattice light-sheet microscopy (Planchon et al., 2011; Chen et al., 2014) offer excellent spatial resolution on the order of 300 nm; however, these techniques achieve high resolution by constructing very thin light-sheets over a short field-of-view (typically with a length of around 100  $\mu\text{m}$ ). Covering a zebrafish larval brain with a lateral cross-section of  $800 \times 600 \mu\text{m}^2$  would thus require extensive tiling, since it is physically not possible to create such thin sheets of light over larger field-of-views with a reasonable illumination power density. Even if a different, yet-to-be-identified physical approach would enable the construction of light-sheets with such properties in the future, such microscopes would still intrinsically be too slow for most functional imaging applications: imaging a 200  $\mu\text{m}$  deep brain volume with a 300 nm thick light sheet would require acquiring on the order of 1,000 images to achieve sufficiently high z-sampling, i.e.  $\sim$ 10-fold more images than are needed for conventional illumination strategies using thicker light sheets. In order to overcome these limitations and provide high spatial resolution and high temporal resolution at the same time, the multi-view imaging techniques diSPIM and IsoView have been developed (Wu

et al., 2013; Chhetri et al., 2015). As discussed earlier, IsoView microscopy offers an imaging mode that is particularly well-suited to functional imaging applications: this mode relies on the use of thick light sheets to maximize temporal resolution while performing simultaneous acquisition of four orthogonal views to maximize spatial resolution. This spatial-resolution enhancing mechanism does not sacrifice temporal resolution and is also not limited to small volumes.

Importantly, the increase in spatial resolution offered by techniques such as IsoView and diSPIM is critical for cellular resolution imaging of the whole brain of a zebrafish larva or an entire *Drosophila* larva. Conventional light-sheet microscopy utilizing piezo-based volumetric imaging already struggles with cellular resolution imaging in deep regions of the brain and thus suffers from a significant reduction in single-cell coverage (Ahrens et al., 2013). This situation is even worse with extended depth of field imaging techniques such as SPED which degrade not only lateral resolution but also suffer from a more than 2-fold decrease in axial resolution (Tomer et al., 2015). For an imaging technique with anisotropic PSF, this latter dimension is the most critical factor influencing the ability to perform cellular resolution imaging. A careful analysis of imaging speed and spatial resolution requirements is thus essential to decide on the optimal imaging technique for a given experiment.

When imaging large, multi-cellular organisms spatial resolution can be further improved by using complementary optimization strategies such as adaptive imaging and adaptive optics. These imaging strategies adapt the microscope's degrees of freedom to the optical properties of the specimen as a function of space and time, in order to compensate for aberrations and improve the overall geometry between light sheet and detection focal plane. Adaptive light-sheet microscopy suitable for functional imaging already exists (Royer et al., 2016), using design principles that

minimize the number of measurement needed to map out the specimen's optical properties and thus maximize the microscope bandwidth used for functional imaging.

#### *Mode of fluorescence excitation and imaging geometry*

Complementary to these performance considerations in the domain of temporal and spatial resolution, certain types of functional imaging experiments introduce additional technical requirements and constraints. For example, behavioral assays using visual stimulation may require the use or exclusion of certain wavelengths for whole-brain functional imaging, so as not to disrupt the behavior under investigation. This type of requirement can be effectively addressed e.g. by using two-photon excitation. However, one needs to consider that signal rates in two-photon light-sheet microscopy are lower than in one-photon light-sheet microscopy, which impacts signal-to-noise ratio and imaging speed. A side-by-side comparison in *Drosophila* larval CNS explants with hs-SiMView light-sheet microscopy showed that a volume rate of 2 Hz marks the upper limit of two-photon functional imaging in this specimen when striving for image data with a signal-to-noise ratio suitable for automated, quantitative computational analyses (Lemon et al., 2015). By contrast, one-photon functional imaging still offered high image quality at volume rates of 5 Hz and was ultimately limited by camera speed rather than the signal rate. As discussed above, two-photon light-sheet imaging has also been very successfully demonstrated for the zebrafish larval brain (Wolf et al., 2015). Since the field-of-view is even larger in this scenario (which in turn reduces signal rate when using two-photon excitation at a given illumination power density), imaging speed was limited to 1 Hz for a subset of the total brain volume, enabling the acquisition of 10 images per second at a 100 ms exposure time per frame (which is contrasted by the ~1 ms exposure time per frame usually used for whole-brain functional imaging with one-photon excitation). When using two-photon excitation it is furthermore important to avoid tissue regions

exhibiting pigmentation, as high light absorption at infrared wavelengths in these regions typically results in severe photo-damage of pigment-producing cells.

Finally, we note that the decision on the optimal imaging assay also depends on the level of optical access offered by the specimen. Although multi-objective light-sheet microscopes generally offer the highest image quality and highest spatial resolution (for the reasons discussed above), these optical geometries necessitate access to the specimen from at least two orthogonal directions. While this does not represent a practical constraint for most model systems, such as *C. elegans*, *D. melanogaster* and zebrafish, it is a prohibitive limitation for *in vivo* imaging of the mouse brain. SCAPE microscopy, which facilitates illumination and detection via a single objective, offers an excellent solution for functional imaging in this model system (Bouchard et al., 2015).

#### 4.5 Processing and Analysis of Light-Sheet Functional Imaging Data

Light-sheet whole-brain or whole-CNS functional image data sets are typically relatively large and encode detailed information about complex dynamic processes across the nervous system. The sheer size and complexity of these images thus introduce substantial challenges for post-acquisition data management and data analysis. In this section, we will discuss the key computational steps involved in the analysis of functional image data acquired with state-of-the-art light-sheet microscopy (**Figure 7**).

A typical 1-hour whole-brain functional recording at 4 Hz in larval zebrafish using SiMView light-sheet microscopy (Tomer et al., 2012; Ahrens et al., 2013; Lemon et al., 2015) comprises 14,400 image stacks with a size of 246 MB each (2048 x 1536 x 41 voxels, corresponding to a volume of 800 x 600 x 200  $\mu\text{m}^3$ ) or 3.4 TB in total. Typical data volumes are similar for other model systems and other light-sheet microscope implementations: A 4.5-hour whole-CNS functional recording at

2 Hz in embryonic/larval *Drosophila* using IsoView microscopy (Chhetri et al., 2015) consists of 32,400 time points comprising four image stacks each with a size of 84 MB per stack (four orthogonal views, 1728 x 728 x 35 voxels, corresponding to a volume of 700 x 300 x 170  $\mu\text{m}^3$ ) or 10.4 TB in total. In both examples, calcium dynamics are recorded simultaneously for a fairly large number of neurons – more than 10,000 in early *Drosophila* first instar larvae and approximately 100,000 across the zebrafish larval brain.

The first key requirement for data sets of this size is an appropriate data handling and storage solution, in particular if such experiments are performed on a daily basis. An effective hardware and software solution is not only important for long-term data storage but also for computational efficiency in all subsequent image processing and visualization steps. At the hardware level, image data are typically streamed locally to solid state disks combined in RAID-0 arrays. At the end of each microscopy experiment, the data is then transferred to file servers with relatively inexpensive high-capacity hard disk drives combined in RAID-6 arrays (Ahrens et al., 2013; Chhetri et al., 2015; Lemon et al., 2015). High-capacity file servers capable of storing 500-1,000 TB of raw image data with this level of redundancy can be purchased at a cost of \$80 per TB at the time of writing of this chapter. However, it is usually not practical to store data in an uncompressed file format – this approach would dramatically increase storage costs, reduce data throughput during image processing and introduce overhead during data inspection. Thus, it is highly recommended to use a file format that combines high compression ratios, a lossless compression scheme with high read and write speeds and a data structure that offers access to spatial or temporal sub-regions of the 4D image data with little to no overhead (Amat et al., 2015). This latter strategy of partitioning image data in small 4D data chunks is extremely valuable both for interactive data visualization and for high-throughput image processing: data visualization rarely involves viewing

all of the data at the same time across space and time, and efficient image processing demands that computations are parallelized across the entire data set to the maximum extent possible, which in turn requires distributing chunks of image data to different processing cores. A powerful solution to this problem, which combines all features in a single, open-source file format termed KLB, has been introduced by Amat et al. (Amat et al., 2015) (**Figure 7, Step 1**). KLB offers the same lossless compression ratio as the 3D JPEG2000 format, but improves read and write speeds more than 3-fold. In contrast to JPEG2000, KLB can also take full advantage of modern multi-core processors with large numbers of processing cores and uses a block-based scheme that subdivides large volumetric image data as sets in small data chunks (with freely adjustable spatial and/or temporal dimensions) to form powerful synergies with data visualization and high-throughput image processing tasks.

Before moving on to the main image processing workflow that facilitates the extraction and analysis of the functional signals encoded in the time-lapse image data, additional computational steps are often needed that vary with the type of light-sheet microscopy used for data acquisition. For example, multi-view imaging is a powerful concept (Swoger et al., 2007) that can be harnessed for increasing physical coverage of partially opaque specimens, such as *Drosophila* embryos and larvae (Tomer et al., 2012; Chhetri et al., 2015; Lemon et al., 2015), and for improving spatial resolution (Wu et al., 2013; Chhetri et al., 2015). However, acquiring multi-view image data in turn demands efficient approaches to multi-view image registration, fusion and/or deconvolution to take full advantage of the information encoded in complementary views. Several powerful solutions to this end exist in the form of open-source software packages, including methods for interest-point-based image registration (Preibisch et al., 2010), content-based image registration (Chhetri et al., 2015) and high-throughput 3D multi-view deconvolution that takes full advantage

of modern graphics processing units (GPU) and multi-core central processing units (CPU) (Chhetri et al., 2015) (**Figure 7, Step 1**). The latter software is capable of multi-view deconvolution of 10 TB data sets within about 2 days on an image processing workstation equipped with a high-end CUDA-enabled graphics card in the price range of \$500-1,000.

At the core of a typical analysis pipeline for functional image data are the processing steps that follow the basic data handling and processing tasks described above. These steps typically involve the use of computational approaches to functional image segmentation, regression, dimensionality reduction, clustering and other approaches to mapping of activity across the brain or nervous system (Keller and Ahrens, 2015) (**Figure 7, Step 2**). Since light-sheet based functional imaging has not yet been widely adopted, it is not uncommon that new custom computational tools are developed and used in each new study involving light-sheet microscopy data. We note, however, that several general computational toolkits are already available. In particular, Freeman et al. (Freeman et al., 2014) and Pnevmatikakis et al. (Pnevmatikakis et al., 2016) present methodologies and algorithms to this end that likely form a good starting point for data exploration in many investigations. Moreover, fast and simple software tools for mapping activity at the voxel level across entire nervous systems in response to external stimuli or robust internal events were presented by Lemon et al. (Lemon et al., 2015). This toolkit enabled a systematic, unbiased search for neurons across the *Drosophila* nervous system with distinct and robust activity signatures during different types of motor programs.

Following the in-depth analysis of a given whole-brain or whole-CNS functional imaging data set, it is often desirable to evaluate the robustness and significance of the respective findings across multiple specimens. This final step typically involves the registration of image data or neural activity maps derived from multiple brains or nervous systems in 3D (**Figure 7, Step 3**). Such

computations are usually complicated by the fact that overall geometry and local neuronal morphologies differ significantly across multiple specimens, which in turn demands non-linear registration methods to maximize spatial correspondence of individual neurons or (more realistically) local anatomical regions comprising small populations of neurons across all data sets. Typical processing strategies to this end first construct reference brains or entire reference nervous systems and then map individual data sets onto these reference scaffolds e.g. by taking advantage of non-linear registration algorithms of the open-source framework Advanced Normalization Tools [<https://github.com/stnava/ANTs>]. Example workflows that follow this concept were presented and applied by Lemon et al. (Lemon et al., 2015) for the *Drosophila* larval CNS and by Portugues et al. (Portugues et al., 2014) for the zebrafish larval brain.

#### 4.6 Outlook

The recent advancements in light-sheet imaging discussed in this chapter have opened a window into neuronal imaging in multi-cellular organisms with high spatiotemporal resolution. Light-sheet microscopy for functional neuronal imaging is still in its early days, and we expect further improvements of this technique as some of the still outstanding challenges are addressed.

One obvious set of future advancements in light-sheet imaging will be the mitigation of light scattering and optical aberrations, which manifest themselves as a degradation in image quality at larger imaging depths and impact more severely in non-transparent tissues. Adaptive imaging techniques (Ji et al., 2010; Wang et al., 2015) and automated framework capable of optimizing the image quality across the specimen volume in real-time (Royer et al., 2016) can address some of these issues and thus further complement the imaging capabilities of light-sheet methods. Light-sheet microscopy is also poised to benefit greatly from recently developed clearing methods (Höckendorf et al., 2014; Marx, 2016), which largely mitigate light scattering in *ex vivo* tissues,

and present a unique opportunity to image large tissue volumes. When combined with light-sheet microscopy these approaches offer a way to obtain images of the entire cleared volume at high spatial resolution. It would thus in principle already be feasible with existing methodology to first map activity in a neural tissue or an entire brain/CNS at cellular resolution, then fix and chemically clear the specimen, and finally acquire an anatomical map of the entire tissue with spatial resolution of 100 nm or better, in particular when light-sheet microscopy is paired with the recently developed Expansion Microscopy (ExM) methods (Chen et al., 2015; Chozinski et al., 2016). Combining these high-resolution anatomical and high-speed functional measurements enabled by light-sheet microscopy presents a great opportunity to interpret and understand functional activity patterns in a structural/anatomical context.

Light-sheet microscopy also stands to benefit directly from ongoing advancements in complementary optical tools for neuronal studies, such as the development of red-shifted calcium sensors (Dana et al., 2016), voltage sensors (Peterka et al., 2011), and the expanding optogenetics toolkit (Fenno et al., 2011). As red-shifted calcium sensors make it feasible to image from deeper regions of the brain, high-speed light-sheet microscopes would record neuronal activities at a high spatiotemporal resolution from regions that are typically inaccessible to GFP-based sensors. Additionally, a high-speed, two-color recording from two distinct population of cells would immediately be possible, particularly with light-sheet microscopes that allow simultaneous multi-color imaging, such as the IsoView microscope. The development of voltage sensors with high signal-to-noise ratio, brightness, and photo-stability would enable a way to record the membrane potential directly, and when imaged with high-speed light-sheet microscopes, electrical activity could be systematically measured across a relatively large population of neurons at the same time. Successful large-volume voltage imaging is expected to demand substantial improvements in the

acquisition speed of light-sheet microscopy. Efforts to this end will require further conceptual advances in light-sheet microscopy but will also benefit from the ongoing advancement of sCMOS camera technology and related detector technology. Another avenue of potential future improvements is the integration of high resolution, high-speed volumetric imaging of the nervous system using light-sheet microscopy and the delivery of precise and targeted optogenetics manipulation. An implementation of an online data analysis platform for instructing perturbations, paired with light-sheet microscopy for volumetric imaging at high spatiotemporal resolution would then enable functional connectivity mapping as well as online hypothesis testing in a behaving animal. With the ongoing rapid advancements in light-sheet microscopy and the development of complementary optical tools, we will undoubtedly see a steadily expanding role of light-sheet microscopy in elucidating the function of the nervous system.

## **Figures and Figure Captions**

### **Figure 1:** Main classes of light-sheet microscopy techniques for functional imaging

Overview of the main classes of light-sheet microscopy techniques designed to address the respective challenges associated with functional imaging in various biological model systems. This overview includes a brief summary of the key strengths and reference implementations presented to date for each class.

Figure 1

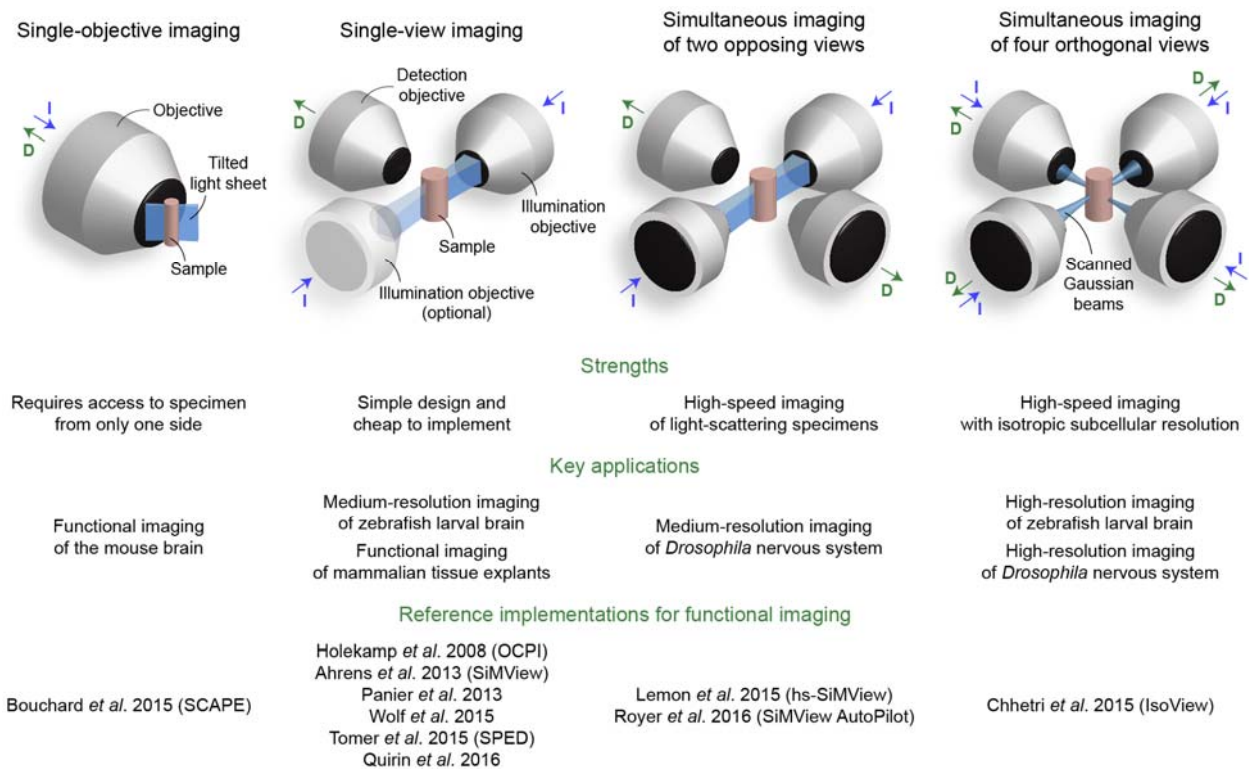


**Figure 2:** Light-sheet microscopy techniques for zebrafish whole-brain functional imaging

Light-sheet microscopy techniques for single-view functional imaging of the zebrafish larval brain by Ahrens et al. 2013 (a-c), Panier et al. 2013 (d-f), Vladimirov et al. 2014 (g-i) and Wolf et al. 2015 (j,k).

- (a) Whole-brain, neuron-level functional imaging in larval zebrafish using laser-scanning light-sheet microscopy (Keller et al., 2008). The zebrafish is embedded in agarose gel and positioned in front of the detection lens. The 4- $\mu\text{m}$ -thick light sheet is generated by fast vertical scanning of a laser beam focused inside the fish by one or both illumination objectives oriented orthogonal to the detection objective. Fluorescence is recorded with a fast sCMOS camera. Volumetric imaging is performed by scanning the light sheet across the sample and moving the detection objective so that the light sheet always coincides with the focal plane (Ahrens et al., 2013).
- (b) Whole-brain, neuron-level activity, reported by a genetically encoded calcium indicator in a week-old Tg(elavl3:GCaMP5G) fish. Panels show lateral and dorsal projections of changes in fluorescence intensity ( $\Delta F/F$ ) at one point in time. Whole-brain volumes were recorded in intervals of 1.39 s.
- (c) Activity at the single-neuron level in a sub-region of a single slice from the volume visualized in (b). Activity is shown superimposed on the anatomy. Slices represent activity recorded at consecutive intervals of 1.39 s.
- (d) Light-sheet microscope design implemented by Panier et al. 2013 for zebrafish whole-brain functional imaging.
- (e) Dorsal and lateral views of the brain-volume reconstructed from a complete 3D stack.
- (f) Enlarged views of the three different sub-regions highlighted by green rectangles in (e).
- (g) Light-sheet microscope design by Vladimirov et al. 2014 for whole-brain functional light-sheet imaging of fictively behaving zebrafish. A larval zebrafish receives visual input from a display underneath, and intended motor output is recorded electrically from the tail. To avoid exposing the eyes to direct laser light, two laser beams are utilized, one scanning from the side but skipping over the eyes, and the second scanning the tissue between the eyes from the front. The detection objective, located above the chamber, is not shown.

(h) Schematic of the laser-scanning strategy in the microscope implementation by Vladimirov et al. 2014.

(i) Whole-brain functional imaging during behavior in a Tg(elavl3:GCaMP6s) fish. The panels show dorsal maximum-intensity projections of  $\Delta F/F$  over the entire volume during stimulus presentation (averaged over 24 trials), superimposed on the anatomical map (gray). Cells and neuropil distributed across the brain show activity during the optomotor response.

(j) Light-sheet microscope implementation by Wolf et al. 2015 for two-photon light-sheet functional imaging of visually evoked neural activity.

(k) Nine images were acquired at 1 Hz across a 5 day old larva brain (90 ms exposure per image), of which four planes are shown here. On the sections shown, the average neural response ( $\Delta F/F$ ), measured in the first second following a  $3,600 \mu\text{W cm}^{-2}$  flash, is color coded (120 flashes, 10 s intervals between flashes).

Panels and captions (a-c) were adapted with permission from Ahrens et al. 2013, (d-f) from Panier et al. 2013, (g-i) from Vladimirov et al. 2014 and (j,k) from Wolf et al. 2015.

Scale bars, 100  $\mu\text{m}$  (b, e, i, k), 10  $\mu\text{m}$  (c, f).

Figure 2

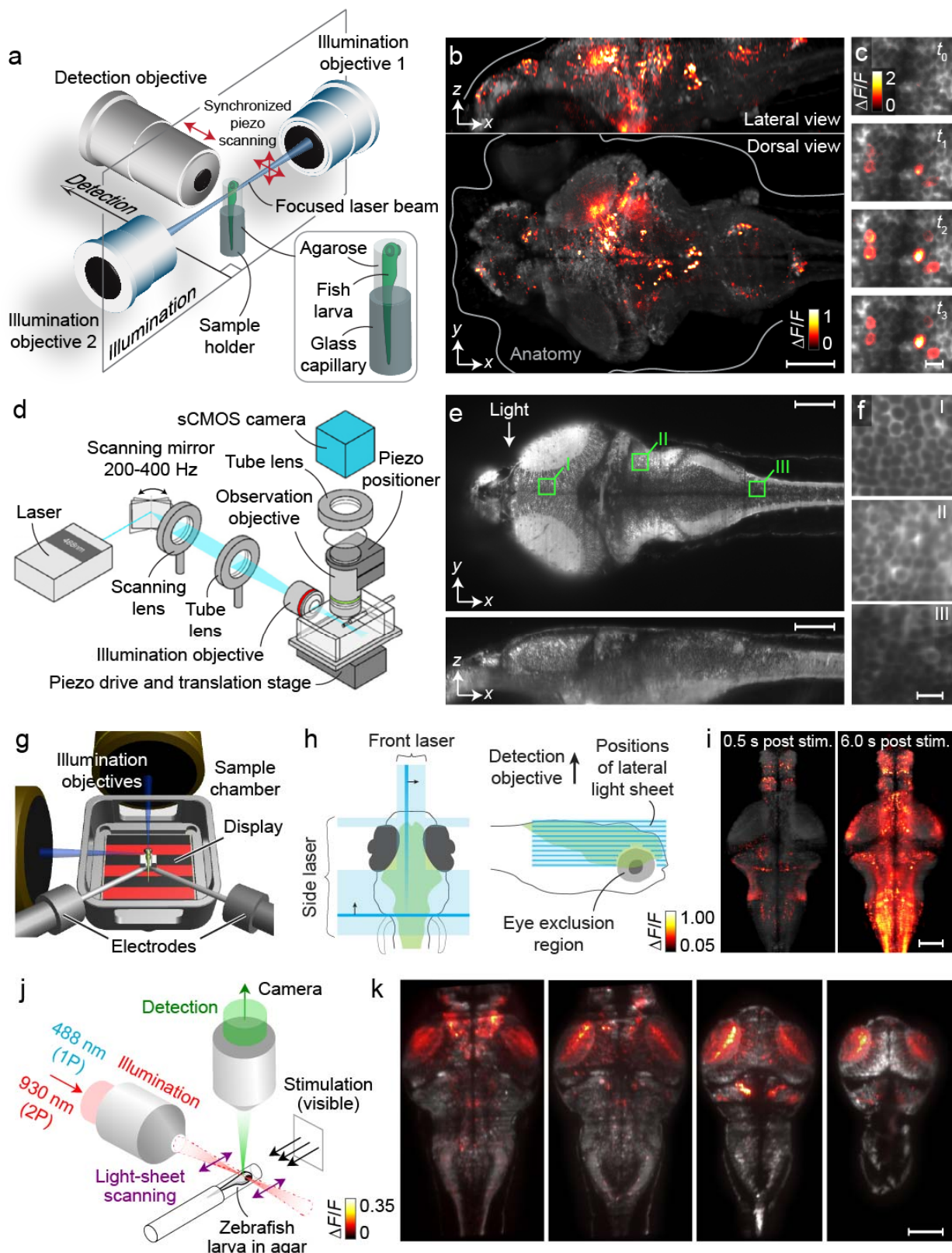


**Figure 3:** Zebrafish functional imaging with axially elongated detection point-spread functions

Light-sheet microscopy techniques with axially elongated detection point-spread functions by Quirin et al. 2016 (a,b) and Tomer et al. 2015 (c,d).

- (a) Schematic of the excitation and imaging path in the technique by Quirin et al. 2016 using cubic phase pupil encoding.
- (b) Demonstration of functional imaging capabilities after data restoration. The images show maximum-intensity projections conveying the spatial specificity of neurons responding to visual motion.
- (c) Schematic of the imaging path in the SPED technique by Tomer et al. 2015. A block of higher (or lower) refractive index ( $n_b$ ) material is placed between the objective and the sample to induce spherical aberrations that elongate the PSF. The thickness of the block is denoted as  $t$ .
- (d) Volume renderings of 10 dpf Tg(elavl3:H2B-GCaMP6s) zebrafish larvae imaged with a 4x/0.28NA objective. Cyan and magenta boxes provide magnified views. Image volumes of 10 consecutive time points were collapsed into one volume by taking the maximum values voxel-wise across the recording duration. The bounding box size is 0.75 mm x 2.99 mm x 0.48 mm.

Panels and captions (a,b) were adapted with permission from Quirin et al. 2016, (c,d) from Tomer et al. 2015.

Scale bar, 100  $\mu\text{m}$  (b).

Figure 3

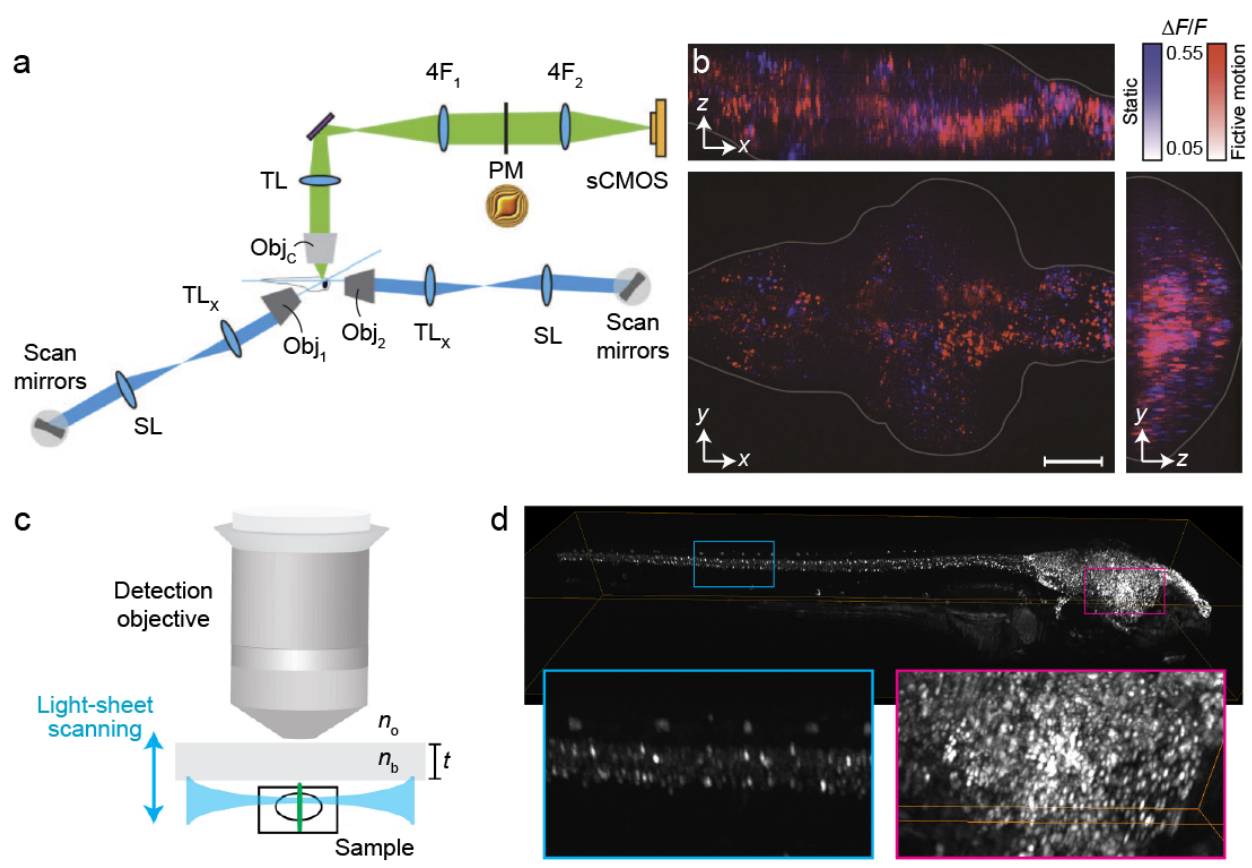


**Figure 4:** Light-sheet microscopy techniques for high-resolution zebrafish whole-brain functional imaging

Light-sheet microscopy techniques by Chhetri et al. 2015 (a-d) and Royer et al. 2016 (e,f) that enable whole-brain functional imaging with high temporal resolution and high spatial resolution.

(a) Isotropic Multiview (IsoView) light-sheet microscopy by Chhetri et al. 2015. The IsoView microscope consists of four orthogonal arms for simultaneous light-sheet illumination and fluorescence detection. The specimen is located at the center of this arrangement. Volumetric imaging consists of sweeping light sheets across the sample and translating detection planes with objective piezo positioners. In the primary mode of IsoView microscope operation, illumination and detection are performed at the same time in all arms, and cross-talk is avoided via spatially matched beam scanning and confocal detection using a phase offset in orthogonal arms (spatial separation).

(b) IsoView whole-brain functional imaging in larval zebrafish. Dorsoventral and lateral projections of IsoView functional imaging data of the brain of a 3-d-old larval zebrafish expressing nuclear-localized GCaMP6 throughout its nervous system.

(c) Side-by-side comparison of conventional image data (acquired using single-view functional imaging, see Figure 2) and multiview deconvolved IsoView image data for x-y, x-z and y-z slices from the two deep-tissue image regions highlighted in (b). Optical path lengths inside the brain relative to lateral and dorsal surfaces were 140  $\mu\text{m}$  and 170  $\mu\text{m}$  for region 1 and 80  $\mu\text{m}$  and 110  $\mu\text{m}$  for region 2.

(d) Side-by-side comparison of intensity profiles in conventional image data and multiview deconvolved IsoView image data for the four linear segments (A1-A2, B1-B2, C1-C2 and D1-D2) indicated in (c). Note that FWHM size measurement results do not directly quantify local resolution, as the results have not been corrected for the finite physical size of the analyzed structures (cell somas typically have a diameter of at least 3  $\mu\text{m}$ ).

(e) Spatiotemporally adaptive light-sheet microscopy by Royer et al. 2016. Overview of the fully automated light-sheet microscopy framework for spatiotemporally adaptive imaging, which consists of (1) a multi-view light-sheet microscope with ten digitally adjustable degrees-of-

freedom that control 3D offsets and 3D angles between light sheets and detection focal planes, and (2) a real-time software layer that autonomously monitors image quality throughout the imaging volume and automatically and continuously adjusts these degrees of freedom to optimize spatial resolution and image quality across the sample in space and time.

(f) Spatiotemporally adaptive whole-brain functional imaging in larval zebrafish. (b) Side-by-side comparison of image quality and spatial resolution in adaptively corrected and uncorrected image data of a representative midbrain region after 11 hours of whole-brain functional imaging in a 4-day old Tg(elav3:GCaMP6f) zebrafish larva. Enlarged views of the image regions marked by orange boxes are shown next to each overview image. Note that non-adaptive imaging fails to resolve individual cell identities, whereas adaptive imaging recovers and maintains single-cell resolution.

Panels and captions (a-d) were adapted with permission from Chhetri et al. 2015, (e,f) from Royer et al. 2016.

Scale bars, 50  $\mu\text{m}$  (b), 5  $\mu\text{m}$  (c,e; f, enlarged views), 20  $\mu\text{m}$  (f, overview images).

Figure 4

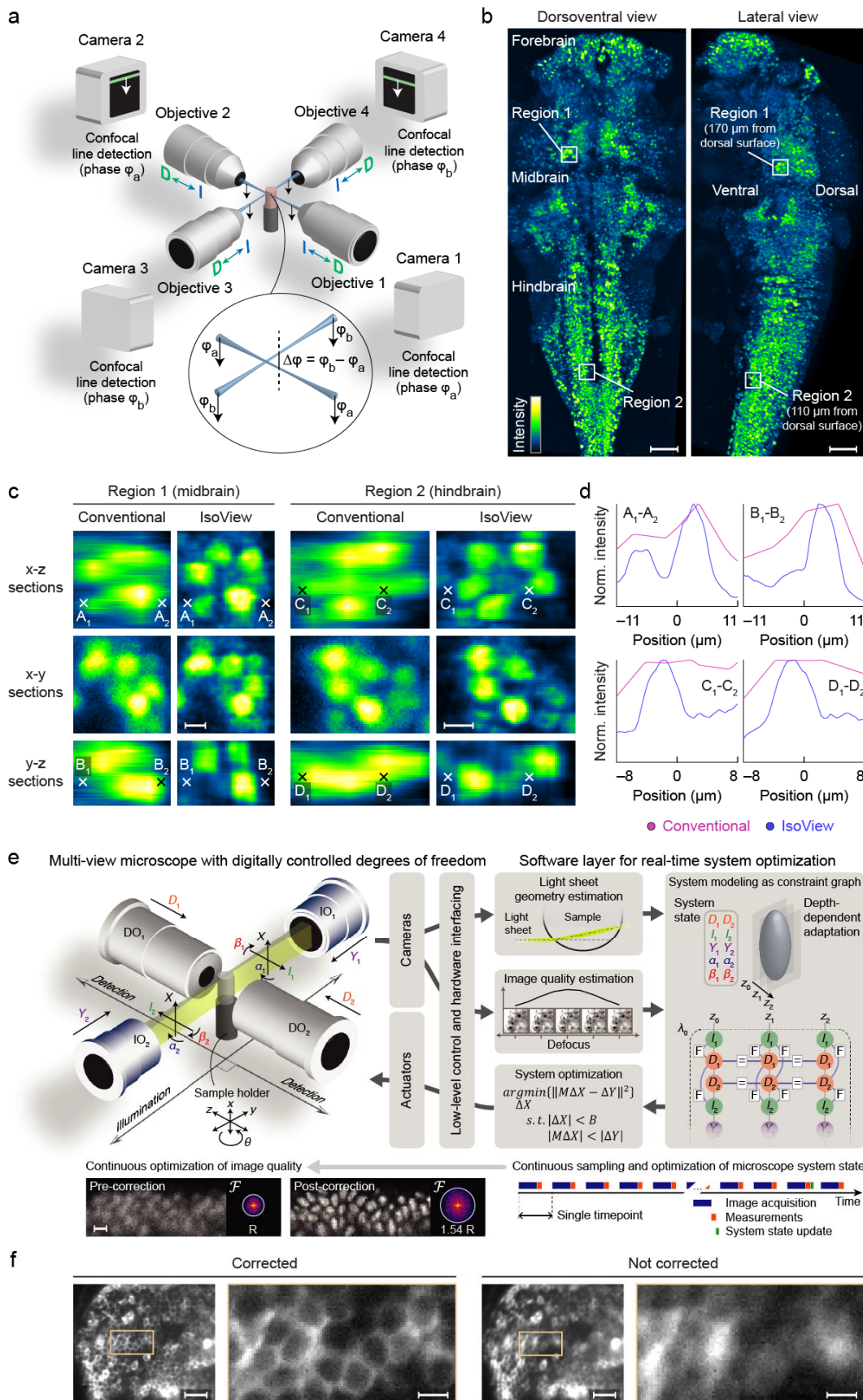


**Figure 5:** Light-sheet microscopy techniques for *Drosophila* whole-CNS functional imaging

Light-sheet microscopy techniques for functional imaging of the *Drosophila* embryonic, larval and adult nervous system by Lemon et al. 2015 (a-d), Chhetri et al. 2015 (e,f) and Liang et al. 2016 (g,h).

(a) hs-SiMView light-sheet microscope design by Lemon et al. 2015 for whole-CNS functional imaging in strongly light-scattering *Drosophila* CNS explants. The illustration shows the hs-SiMView microscope core for functional imaging, including the central specimen chamber, two illumination objectives for bi-directional fluorescence excitation with scanned laser light sheets and two opposing detection objectives mounted on high-speed piezo stages. The 3D volumes covered by the two piezo-operated detection objectives are matched with a precision of a few micrometers using custom Y-Z-theta fine adjustment stages and objective X-flexures.

(b) For optimal optical access, the CNS of a *Drosophila* third instar larva is extracted by surgery and embedded in a soft, transparent agarose cylinder supported by a glass capillary for mounting in the hs-SiMView light-sheet microscope. The CNS explant is then transferred to the microscope's specimen chamber filled with physiological saline.

(c) Whole-CNS functional imaging at 5Hz of a *Drosophila* third instar larval CNS expressing 57C10-GAL4,UAS-GCaMP6s, using hs-SiMView light-sheet microscopy. Imaging was performed with one-photon excitation at 488 nm, maintaining a constant imaging speed of 370 frames per second (491 MB per second) for a period of 1 h. Image panels show maximum-intensity projections of  $\Delta F/F$  (color look-up-table) and CNS anatomy (grey, gamma-corrected GCaMP6s baseline fluorescence) from dorsal (top) and lateral (bottom) views, for five time points during a backward locomotor sequence. Outline indicates CNS boundary.

(d) Image sequence showing changes in  $\Delta F/F$  for cell bodies in the ROI indicated by a white rectangle in panel (c). This example sequence demonstrates slow changes in  $\Delta F/F$  across a bout of locomotor waves. Images are median filtered. ABD, abdomen; BL, brain lobes; SOG, suboesophageal ganglion; TH, thorax.

(e) IsoView whole-animal functional imaging in embryonic *Drosophila* by Chhetri et al. 2015. (a) Dorsal- and lateral-view maximum-intensity projections of multiview deconvolved IsoView

image data of a stage 17 *Drosophila* embryo expressing GCaMP6s throughout the nervous system. The underlying four-view image data were recorded in 800 ms. A false-color look-up table is used for better visibility of high-dynamic-range images.

(f) Improving resolution and isotropy by IsoView functional imaging. Side-by-side comparison of raw anisotropic image data (conventional single-view image data, top and middle rows) and multiview deconvolved IsoView image data (bottom row) for an optical section of the ventral nerve cord of the specimen shown in (e), using the same false-color look-up table. Roman numerals identify locations of somas with high GCaMP6s fluorescence.

(g) Illustration of light-sheet method for long-term *in vivo* imaging of the *Drosophila* adult brain. The head is immersed in saline while the body remains in an air-filled enclosure.

(h) Ca<sup>2+</sup> activity patterns in circadian pacemaker neurons *in vivo*. Left: A representative image of tim>GCaMP6s signals showing the locations of five identifiable pacemaker groups. Right: Representative images showing 24-hour Ca<sup>2+</sup> activity patterns of five identifiable groups.

Panels and captions (a-d) were adapted with permission from Lemon et al. 2015, (e,f) from Chhetri et al. 2015 and (g,h) from Liang et al. 2016.

Scale bars, 50 μm (c,e), 10 μm (d,f), 20 μm (h).

Figure 5

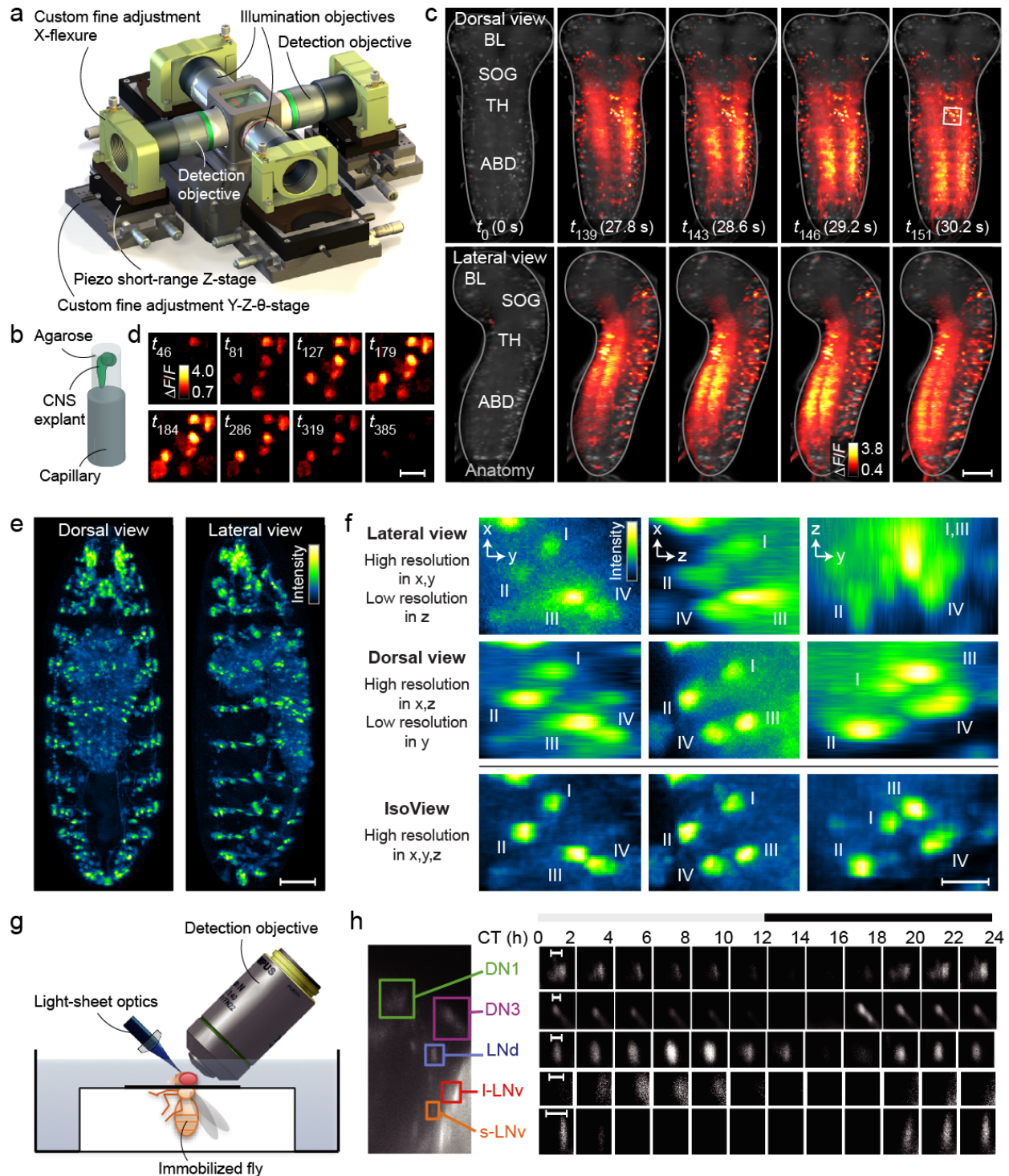


**Figure 6:** Light-sheet microscopy techniques for functional imaging of mammalian neural tissues

Light-sheet microscopy techniques by Holekamp et al. 2008 (a,b) and Bouchard et al. 2015 (c,d) for functional imaging of mammalian neural tissues.

(a) Schematic of an Objective-Coupled Planar Illumination (OCPI) light-sheet microscope by Holekamp et al. 2008. Laser light for fluorescence excitation is provided by an optical fiber and is shaped into a light sheet  $\sim 3\text{--}5 \mu\text{m}$  thick using two lenses. The light sheet is coplanar with the focal plane of the detection objective. By coupling the illumination optics to the objective lens, the alignment of the light sheet with the detection focal plane is maintained while scanning a sample volume using the piezoelectric positioner attached to the detection objective. Objective lens and illumination optics are designed for water immersion applications.

(b) Probing of responses to chemical stimuli of single VNO neurons by high-speed 3D calcium imaging. The image shows a single optical section of an intact VN epithelium labeled with Oregon Green BAPTA-1. Purple dots indicate the positions of single neurons.

(c) Illustration of SCAPE's scanning-descanning geometry by Bouchard et al. 2015, which sweeps an oblique light sheet back and forth across the sample while the descanned detection plane remains stationary. The only moving component is the slowly oscillating polygonal scanning mirror.

(d) SCAPE imaging in an awake, behaving mouse with intravascular Texas red dextran (red) and GCaMP6f in superficial dendrites from layer 5 neurons (green). The images show individual  $x'$ – $y'$  planes extracted from a single  $350 \times 800 \times 105 \mu\text{m}$  ( $x'$ – $y'$ – $z'$ ) SCAPE volume acquired in 0.1 s (each plane is an average of five sequential time points).

Panels and captions (a,b) were adapted with permission from Holekamp et al. 2008 and (c,d) from Bouchard et al. 2015.

Scale bars, 50  $\mu\text{m}$  (b), 100  $\mu\text{m}$  (d).

Figure 6

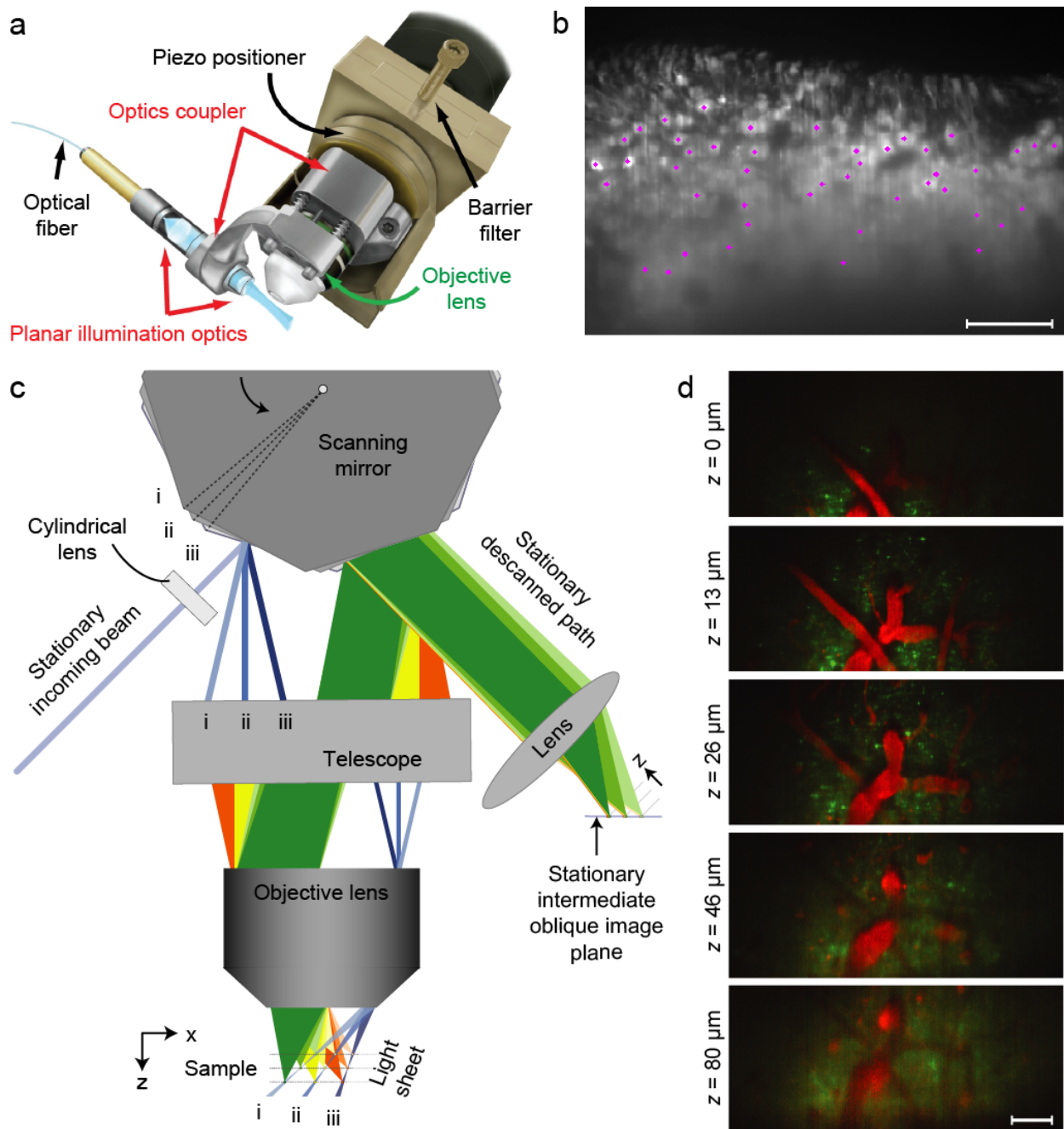


**Figure 7:** Processing and analysis of light-sheet functional image data

Overview of key computational steps in the processing and analysis of large-scale light-sheet functional image data, categorized as “basic image processing” (step 1, top), “extracting quantitative information from images” (step 2, middle) and “analyzing robustness of results” (step 3, bottom). From top to bottom, this overview figure includes methodological examples from the studies listed below.

Multi-view registration and deconvolution (Chhetri et al., 2015): Images show maximum-intensity projections of single- and multi-view deconvolved IsoView image data of a stage 17 *Drosophila* embryo expressing GCaMP6s throughout the nervous system. Computations were performed using a high-throughput GPU-based implementation of the Lucy-Richardson algorithm, which achieves a data throughput of 1 Gigavoxel per minute (including I/O) on Tesla K40 GPUs when executing 20 iterations of the algorithm.

Efficient large-scale data management (Amat et al., 2015): The Keller Lab Block (KLB) lossless image compression format combines high compression ratios, fast read/write speeds and a flexible block architecture that enables efficient access to arbitrary regions of interest. Inspired by Parallel BZip2, a common Linux compression module, images are partitioned in 5D blocks and all blocks are compressed in parallel using BZip2. Both reading and writing operations are parallelized and scale linearly with the number of cores in the CPU. The KLB source code is accompanied by a simple API for interfacing the open-source C++ code with various platforms, as well as an interface file for the SWIG tool, which can be used to autogenerate wrapper code for various languages, including Java, C#, Python, Perl and R.

Mapping whole-brain neural activity (Freeman et al., 2014): Analysis of direction tuning across the brain of larval zebrafish presented with moving whole-field visual stimuli in a setup that combines light-sheet imaging with visual stimulation and behavior (Vladimirov et al., 2014). The direction tuning maps are derived by fitting every voxel (with ~100 voxels per neuron) with a tuning-curve model that separately describes the temporal response profile and the tuning to direction. Color indicates preferred direction; saturation, tuning width (i.e., circular variance); brightness, response strength. White means responsive, but without unidirectional tuning. Image shows a dorsal maximum intensity projection through 39 planes covering 195  $\mu\text{m}$ .

Mapping whole-brain neural activity (Lemon et al., 2015): Mapping whole-CNS activity timing for forward and backward locomotor waves (dorsoventral and lateral slices are shown to the left and right, respectively). To create these maps, the timing of activity was evaluated across all detected wave events in one specimen (forward:  $n = 30$ , backward:  $n = 70$ ). Intuitively, these maps show, for each part for the CNS, the time during locomotor wave windows when activity increases. Arrows mark relative progression of locomotor waves on dorsal/ventral sides of the VNC (ascending numbers). Forward and backward wave window sizes were defined as [-10 s, 10 s] and [-6 s, 2 s] (centered on waves in ventral nerve cord) to ensure wave propagation was captured throughout the ventral nerve cord and overlap of events was avoided.

Neuron identification and activity extraction (Pnevmatikakis et al., 2016): Demonstration of a method for simultaneously identifying the locations of neurons, demixing spatially overlapping components, and denoising and deconvolving the spiking activity from the slow dynamics of the calcium indicator. The method was applied to mouse *in vivo* GCaMP6s data. The top panel shows contour plots of inferred spatial components superimposed on the correlation image of the raw data. The components are sorted in decreasing order based on the maximum temporal value and their size. Contour plots of the first 200 identified components are shown, and the first 36 components are numbered. The bottom panel shows extracted  $\Delta F/F$  fluorescence traces for the first 36 components.

Registration and joint analysis of multiple nervous systems (Lemon et al., 2015): Spatial registration of the nervous systems of six *Drosophila* larvae. All CNS explants used for functional imaging expressed GCaMP panneuronally (57C10-GAL4,UAS-GCaMP6s, shown in green) and tdTomato in anatomically defined regions within the larval CNS (58B03-LexA,LexOP-tdTomato, shown in magenta; expression in mushroom bodies and neuropil regions). To register nervous systems, a CNS template (shown to the right) was constructed from GCaMP reference image stacks representing each of the six independent time-lapse experiments. Image data from each experiment was then registered to the CNS reference template using nonlinear spatial registration techniques.

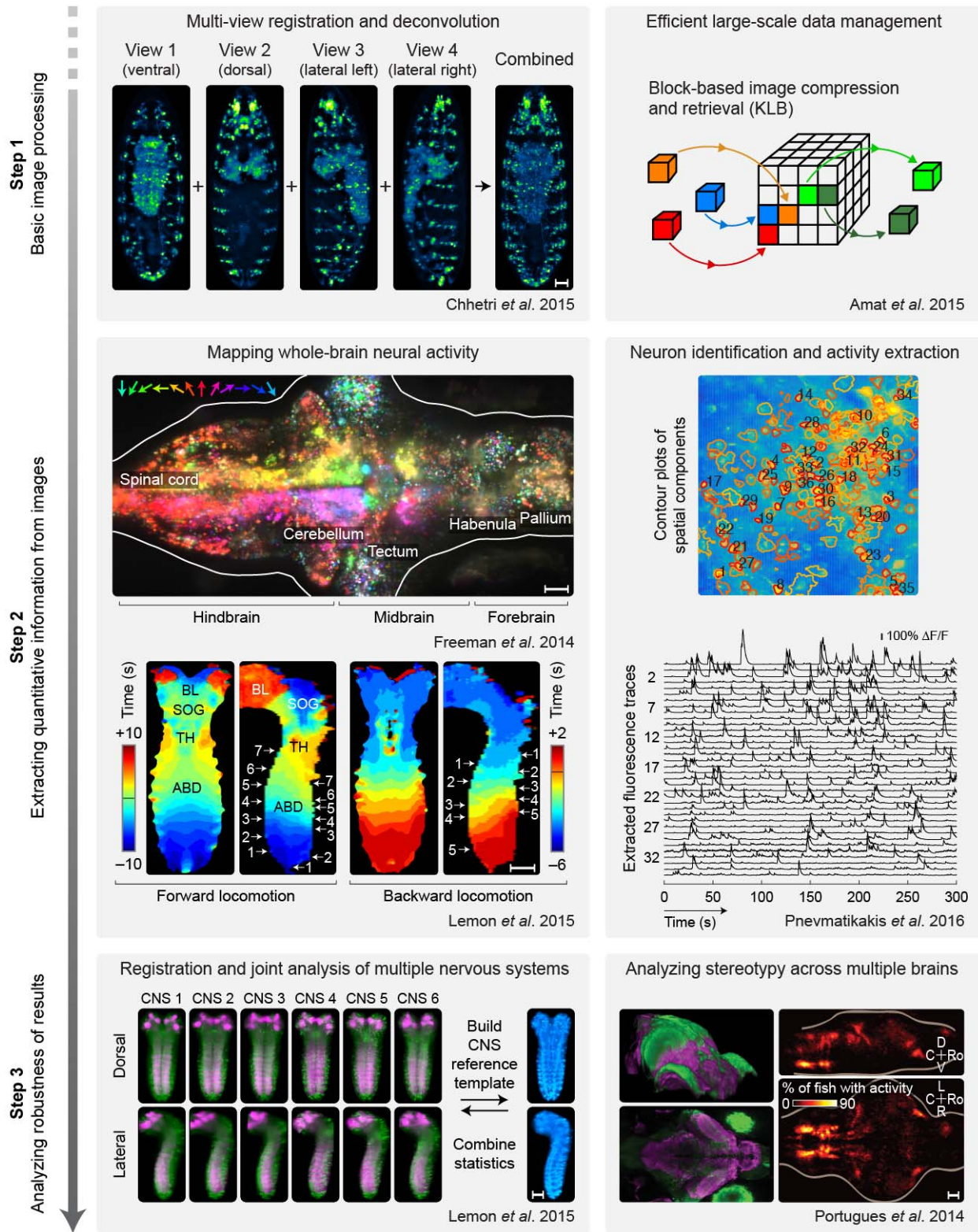
Analyzing stereotypy across multiple brains (Portugues et al., 2014): Three-dimensional volume registration across larval zebrafish brains. Left: An individual brain (green) is morphed onto a reference brain (magenta) by performing an affine transformation, followed by non-rigid

alignment. Right: Spatial maps encoding the percentage of fish ( $n = 13$ ) imaged that show activity at each voxel (after registration) for all voxels within the brain, depicted as maximum projections from two orthogonal views.

All figures and captions were adapted with permission from the respective sources listed in the bottom right corner of each panel.

Scale bars, 30  $\mu\text{m}$  (step 1, left), 40  $\mu\text{m}$  (step 2, top left), 50  $\mu\text{m}$  (step 2, bottom left; step 3).

Figure 7



## References

- Ahrens MB, Orger MB, Robson DN, Li JM, Keller PJ (2013) Whole-brain functional imaging at cellular resolution using light-sheet microscopy. *Nat Methods* 10:413–420.
- Amat F, Höckendorf B, Wan Y, Lemon WC, McDole K, Keller PJ (2015) Efficient processing and analysis of large-scale light-sheet microscopy data. *Nat Protoc* 10:1679–1696.
- Bouchard MB, Voleti V, Mendes CS, Lacefield C, Grueber WB, Mann RS, Bruno RM, Hillman EMC (2015) Swept confocally-aligned planar excitation (SCAPE) microscopy for high-speed volumetric imaging of behaving organisms. *Nat Photonics* 9:113–119.
- Chen B-C et al. (2014) Lattice light-sheet microscopy: Imaging molecules to embryos at high spatiotemporal resolution. *Science* 346:1257998.
- Chen F, Tillberg PW, Boyden ES (2015) Expansion microscopy. *Science* 347:543–548.
- Chhetri RK, Amat F, Wan Y, Höckendorf B, Lemon WC, Keller PJ (2015) Whole-animal functional and developmental imaging with isotropic spatial resolution. *Nat Methods* 12:1171–1178.
- Chozinski TJ, Halpern AR, Okawa H, Kim H-J, Tremel GJ, Wong ROL, Vaughan JC (2016) Expansion microscopy with conventional antibodies and fluorescent proteins. *Nat Methods*:1–7.
- Dana H, Mohar B, Sun Y, Narayan S, Gordus A, Hasseman JP, Tsegaye G, Holt GT, Hu A, Walpita D, Patel R, Macklin JJ, Bargmann CI, Ahrens MB, Schreiter ER, Jayaraman V, Looger LL, Svoboda K, Kim DS (2016) Sensitive red protein calcium indicators for imaging neural activity. *Elife* 5:e12727.
- Dowski ER, Cathey WT (1995) Extended depth of field through wave-front coding. *Appl Opt* 34:1859–1866.
- Fahrbach FO, Voigt FF, Schmid B, Helmchen F, Huisken J (2013) Rapid 3D light-sheet microscopy with a tunable lens. *Opt Express* 21:21010.
- Fenno L, Yizhar O, Deisseroth K (2011) The Development and Application of Optogenetics. *Annu Rev Neurosci* 34:389–412.

- Freeman J, Vladimirov N, Kawashima T, Mu Y, Sofroniew NJ, Bennett D V, Rosen J, Yang C-T, Looger LL, Ahrens MB (2014) Mapping brain activity at scale with cluster computing. *Nat Methods* 11:941–950.
- Fuchs E, Jaffe J, Long R, Azam F (2002) Thin laser light sheet microscope for microbial oceanography. *Opt Express* 10:145–154.
- Grewé B, Langer D, Kasper H, Kampa BM, Helmchen F (2010) High-speed in vivo calcium imaging reveals neuronal network activity with near-millisecond precision. *Nat Methods* 7:399–405.
- Hammen GF, Turaga D, Holy TE, Meeks JP (2014) Functional organization of glomerular maps in the mouse accessory olfactory bulb. *Nat Neurosci* 17:953–961.
- Höckendorf B, Lavis LD, Keller PJ (2014) Making biology transparent. *Nat Biotechnol* 32:1104–1105.
- Holekamp TF, Turaga D, Holy TE (2008) Fast Three-Dimensional Fluorescence Imaging of Activity in Neural Populations by Objective-Coupled Planar Illumination Microscopy. *Neuron* 57:661–672.
- Huisken J, Swoger J, Del Bene F, Wittbrodt J, Stelzer EHK (2004) Optical sectioning deep inside live embryos by selective plane illumination microscopy. *Science* 305:1007–1009.
- Ji N, Milkie DE, Betzig E (2010) Adaptive optics via pupil segmentation for high-resolution imaging in biological tissues. *Nat Methods* 7:141–147.
- Keller PJ, Ahrens MB (2015) Visualizing Whole-Brain Activity and Development at the Single-Cell Level Using Light-Sheet Microscopy. *Neuron* 85:462–483.
- Keller PJ, Schmidt AD, Wittbrodt J, Stelzer EHK (2008) Reconstruction of zebrafish early embryonic development by scanned light sheet microscopy. *Science* 322:1065–1069.
- Lemon WC, Pulver SR, Höckendorf B, McDole K, Branson K, Freeman J, Keller PJ (2015) Whole-central nervous system functional imaging in larval *Drosophila*. *Nat Commun* 6:7924.
- Levoy M, Ng R, Adams A, Footer M, Horowitz M (2006) Light field microscopy. *ACM Trans*

Graph 25:924.

- Liang X, Holy TE, Taghert PH (2016) Synchronous Drosophila circadian pacemakers display nonsynchronous Ca<sup>2+</sup> rhythms in vivo. *Science* 351:976–981.
- Looger LL, Griesbeck O (2012) Genetically encoded neural activity indicators. *Curr Opin Neurobiol* 22:18–23.
- Marx V (2016) Optimizing probes to image cleared tissue. *Nat Methods* 13:205–209.
- Mouroulis P (2008) Depth of field extension with spherical optics. *Opt Express* 16:12995–13004.
- Osten P, Margrie TW (2013) Mapping brain circuitry with a light microscope. *Nat Methods* 10:515–523.
- Panier T, Romano S a, Olive R, Pietri T, Sumbre G, Candelier R, Debrégeas G (2013) Fast functional imaging of multiple brain regions in intact zebrafish larvae using Selective Plane Illumination Microscopy. *Front Neural Circuits* 7:65.
- Peterka DS, Takahashi H, Yuste R (2011) Imaging Voltage in Neurons. *Neuron* 69:9–21.
- Pitrone PG, Schindelin J, Stuyvenberg L, Preibisch S, Weber M, Eliceiri KW, Huisken J, Tomancak P (2013) OpenSPIM: an open-access light-sheet microscopy platform. *Nat Methods* 10:598–599.
- Planchon TA, Gao L, Milkie DE, Davidson MW, Galbraith JA, Galbraith CG, Betzig E (2011) Rapid three-dimensional isotropic imaging of living cells using Bessel beam plane illumination. *Nat Methods* 8:417–423.
- Pnevmatikakis EA, Soudry D, Gao Y, Machado TA, Merel J, Pfau D, Reardon T, Mu Y, Lacefield C, Yang W, Ahrens M, Bruno R, Jessell TM, Peterka DS, Yuste R, Paninski L (2016) Simultaneous Denoising, Deconvolution, and Demixing of Calcium Imaging Data. *Neuron*:285–299.
- Portugues R, Feierstein CE, Engert F, Orger MB (2014) Whole-brain activity maps reveal stereotyped, distributed networks for visuomotor behavior. *Neuron* 81:1328–1343.
- Preibisch S, Saalfeld S, Schindelin J, Tomancak P (2010) Software for bead-based registration of

- selective plane illumination microscopy data. *Nat Methods* 7:418–419.
- Prevedel R, Yoon Y-G, Hoffmann M, Pak N, Wetzstein G, Kato S, Schrödel T, Raskar R, Zimmer M, Boyden ES, Vaziri A (2014) Simultaneous whole-animal 3D imaging of neuronal activity using light-field microscopy. *Nat Methods* 11:727–730.
- Quirin S, Vladimirov N, Yang C-T, Peterka DS, Yuste R, Ahrens M (2016) Calcium imaging of neural circuits with extended depth-of-field light-sheet microscopy. *Opt Lett* 41:855.
- Royer LA, Lemon WC, Chhetri RK, Wan Y, Coleman M, Myers E, Keller PJ (2016) Real-Time Adaptive Light-Sheet Microscopy Recovers High Resolution in Large Living Organisms. *Nat Biotechnol.* (*In Press*)
- Siedentopf H, Zsigmondy R (1902) Über Sichtbarmachung und Größenbestimmung ultramikroskopischer Teilchen, mit besonderer Anwendung auf Goldrubiingläser. *Ann Phys* 315:1–39.
- Sofroniew NJ, Flickinger D, King J, Svoboda K (2016) A large field of view two-photon mesoscope with subcellular resolution for *in vivo* imaging. *Elife* 5:1–20.
- Swoger J, Verveer P, Greger K, Huisken J, Stelzer EHK (2007) Multi-view image fusion improves resolution in three-dimensional microscopy. *Opt Express* 15:8029–8042.
- Tomer R, Khairy K, Amat F, Keller PJ (2012) Quantitative high-speed imaging of entire developing embryos with simultaneous multiview light-sheet microscopy. *Nat Methods* 9:755–763.
- Tomer R, Lovett-barron M, Kauvar I, Broxton M, Deisseroth K (2015) SPED Light Sheet Microscopy : Fast Mapping of Biological System Structure and Function Resource SPED Light Sheet Microscopy : Fast Mapping of Biological System Structure and Function. *Cell* 163:1796–1806.
- Turaga D, Holy TE (2012) Organization of Vomeronasal Sensory Coding Revealed by Fast Volumetric Calcium Imaging. *J Neurosci* 32:1612–1621.
- Vladimirov N, Mu Y, Kawashima T, Bennett D V, Yang C-T, Looger LL, Keller PJ, Freeman J, Ahrens MB (2014) Light-sheet functional imaging in fictively behaving zebrafish. *Nat*

- Methods 11:883–884.
- Voie AH, Bruns DH, Spelman FA (1993) Orthogonal-plane fluorescence optical sectioning: Three-dimensional imaging of macroscopic biological specimens. *J Microsc* 170:229–236.
- Wang K, Sun W, Richie CT, Harvey BK, Betzig E, Ji N (2015) Direct wavefront sensing for high-resolution *in vivo* imaging in scattering tissue. *Nat Commun* 6:7276.
- Wilt BA, Burns LD, Wei Ho ET, Ghosh KK, Mukamel EA, Schnitzer MJ (2009) Advances in Light Microscopy for Neuroscience. *Annu Rev Neurosci* 32:435–506.
- Wolf S, Supatto W, Debrégeas G, Mahou P, Kruglik SG, Sintes J-M, Beaurepaire E, Candelier R (2015) Whole-brain functional imaging with two-photon light-sheet microscopy. *Nat Methods* 12:379–380.
- Wu Y, Wawrzusin P, Senseney J, Fischer RS, Christensen R, Santella A, York AG, Winter PW, Waterman CM, Bao Z, Colón-Ramos D a, McAuliffe M, Shroff H (2013) Spatially isotropic four-dimensional imaging with dual-view plane illumination microscopy. *Nat Biotechnol* 31:1032–1038.
- Xu PS, Lee D, Holy TE (2016) Experience-dependent plasticity drives individual and sex differences in pheromone-sensing neurons. *Neuron*. (*In Press*)
- Yang Z, Haslehurst P, Scott S, Emptage N, Dholakia K (2016) A compact light-sheet microscope for the study of the mammalian central nervous system. *Sci Rep* 6:26317.
- Zalevsky Z, Ben-Yaish S (2007) Extended depth of focus imaging with birefringent plate. *Opt Express* 15:7202–7210.

**Table 1:** Comparison of functional imaging experiments performed with different light-sheet microscopy methods

Imaging Method		hs-SiMView		IsoView		SPED	2P LSFM	SCAPE	OCPI
Reference		Lemon <i>et al.</i> 2015		Chhetri <i>et al.</i> 2015		Tomer <i>et al.</i> 2015	Wolf <i>et al.</i> 2015	Bouchard <i>et al.</i> 2015	Holekamp <i>et al.</i> 2008
Experiment		Whole-CNS Functional Imaging		Whole-Animal Functional Imaging	Whole-Brain Functional Imaging	Whole-Brain Functional Imaging	Functional Imaging of Brain Regions	Functional Imaging of Brain Regions	Functional Imaging of Brain Regions
Model System		<i>Drosophila</i> Third-Instar Larval CNS Explant		<i>Drosophila</i> First-Instar Larva	Larval Zebrafish	Larval Zebrafish	Larval Zebrafish	Mouse	Mouse VNO Explant
Imaging Geometry		Two Illumination Arms Two Detection Arms		Four Illumination Arms Four Detection Arms		One Illumination Arm One Detection Arm	One Illumination Arm One Detection Arm	Single Objective	One Illumination Arm One Detection Arm
Fluorescence Excitation		One-Photon	Two-Photon	One-Photon		One-Photon	Two-Photon	One-Photon	One-Photon
Detection Optics	Detection Objective Manufacturer		Nikon		Special Optics		Olympus	Olympus	Olympus
	Detection Magnification		16x		16x		4x	20x	20x
	Detection Numerical Aperture		0.8		0.714		0.28	1.0	1.0
	Relative Photon Efficiency <sup>1)</sup>		0.64		0.51		0.08	1	1
Resolution	Sampling-Limited System Resolution <sup>2)</sup>	X [µm]	0.8	0.8		3.25	0.8	5.0	2.6
		Y [µm]	0.8	0.8		3.25	0.8	6.5	2.6
		Z [µm]	8.0	0.8		10.0	16.0	6.6	10.0
Relative 3D Resolution <sup>3)</sup>		10		1		206	20	419	132
3D Resolution Anisotropy <sup>4)</sup>		9.0		0		2.1	19.0	0.3	2.8
Volume	Image Size [pixels]		1,216 x 572	1472 x 700	1,504 x 704	2,043 x 1,231	554 x 246	2,048 x 2,048	240 x 200
	Volume Size	X [µm]	494	598	610	830	900	800	600
		Y [µm]	232	284	290	500	400	800	650
		Z [µm]	180	220	210	400	200	72	134
Speed	Acquisition Speed [10 <sup>6</sup> voxels s <sup>-1</sup> ]		257	185	296	674	65	38	19
	Acquisition Speed <sup>5)</sup> [volumes s <sup>-1</sup> ]		2 x 5	2 x 2	4 x 2	4 x 1	12	1	10
									0.2

Footnotes:

- <sup>1)</sup> The photon collection efficiency is proportional to the square of the numerical aperture (NA) and is normalized to the value obtained with the highest-NA (1.0) objective in this table. Note that absolute photon efficiency is affected by additional factors and depends on experiment-specific settings.
- <sup>2)</sup> Sampling-limited resolution considers not only the size of the point-spread-function but also the three-dimensional size of voxels in the image data. According to the Nyquist sampling theorem, effective resolution in each dimension cannot be better than two times the voxel size along the respective dimension. The long axial step size between image planes in hs-SiMView, SPED, 2P LSFM, SCAPE and OCPI experiments is a key factor limiting effective axial resolution for these methods.
- <sup>3)</sup> Three-dimensional (3D) resolution is defined as the product of resolution values in x-, y- and z-dimensions and is normalized to the value obtained for the highest-resolution technique (IsoView).
- <sup>4)</sup> Resolution anisotropy is defined as the ratio of sampling-limited resolution values along those dimensions exhibiting the lowest and highest spatial resolution, respectively, minus one. Thus, if sampling-limited resolution is identical in all dimensions, resolution anisotropy is zero.
- <sup>5)</sup> For microscopes that acquire multiple views of the full specimen volume simultaneously (hs-SiMView, IsoView), acquisition speed is listed as [number of views] x [volume acquisition rate].